

1 **Optimizing sampling strategies in high-resolution paleoclimate records**

2

3 Niels J. de Winter^{1,2} *, Tobias Agterhuis¹, Martin Ziegler¹

4

5 ¹Department of Earth Sciences, Utrecht University, Princetonlaan 8a, 3584 CB Utrecht, the Netherlands

6 ²AMGC research group, Vrije Universiteit Brussel, Pleinlaan 2, 1050 Brussels, Belgium

7

8 Correspondence to: Niels J. de Winter (n.j.dewinter@uu.nl)

9

10 **Abstract**

11 The aim of paleoclimate studies resolving climate variability from noisy proxy records can in essence be
12 reduced to a statistical problem. The challenge is to extract meaningful information about climate variability
13 from these records by reducing measurement uncertainty through combining measurements for proxies
14 while retaining the temporal resolution needed to assess the timing and duration of variations in climate
15 parameters. In this study, we explore the limits of this compromise by testing different methods for
16 combining proxy data (smoothing, binning and sample size optimization) on a particularly challenging
17 paleoclimate problem: resolving seasonal variability in stable isotope records. We test and evaluate the
18 effects of changes in the seasonal temperature and the hydrological cycle as well as changes in accretion
19 rate of the archive and parameters such as sampling resolution and age model uncertainty on the reliability
20 of seasonality reconstructions based on clumped and oxygen isotope analyses in 33 real and virtual
21 datasets. Our results show that strategic combinations of clumped isotope analyses can significantly
22 improve the accuracy of seasonality reconstructions compared to conventional stable oxygen isotope
23 analyses, especially in settings where the isotopic composition of the water is poorly constrained.
24 Smoothing data using a moving average often leads to an apparent dampening of the seasonal cycle,
25 significantly reducing the accuracy of reconstructions. A statistical sample size optimization protocol yields
26 more precise results than smoothing. However, the most accurate results are obtained through monthly
27 binning of proxy data, especially in cases where growth rate or water composition cycles obscure the
28 seasonal temperature cycle. Our analysis of a wide range of natural situations reveals that the effect of
29 temperature seasonality on oxygen isotope records almost invariably exceeds that of changes in water
30 composition. Thus, in most cases, oxygen isotope records allow reliable identification of growth seasonality
31 as a basis for age modelling in the absence of independent chronological markers in the record. These
32 specific findings allow us to formulate general recommendations for sampling and combining data in
33 paleoclimate research and have implications beyond the reconstruction of seasonality. We briefly discuss
34 the implications of our results for solving common problems in paleoclimatology and stratigraphy.

35

36 1. Introduction

37 Improving the resolution of climate reconstructions is a key objective in paleoclimate studies because it
38 allows climate variability to be studied on different timescales and sheds light on the continuum of climate
39 variability (Huybers and Curry, 2006). However, the temporal resolution of climate records is limited by the
40 accretion rate (growth or sedimentation rate) of the archive and the spatial resolution of sampling for climate
41 reconstructions, which is a function of the sample size required for a given climate proxy. This tradeoff
42 between sample size and sampling resolution is especially prevalent when using state-of-the-art climate
43 proxies which require large sample sizes, such as the carbonate clumped isotope paleothermometer (Δ_{47} ;
44 see applications in Rodríguez-Sanz et al., 2017; Briard et al., 2020; Caldarescu et al., 2021) or stable
45 isotope ratios in specific compounds or of rare isotopes (e.g. phosphate-oxygen isotopes in tooth apatite,
46 triple oxygen isotopes in speleothems or carbon isotopes of CO₂ in ice cores; Jones et al., 1999; Schmitt
47 et al., 2012; Sha et al., 2020). The challenge of sampling resolution persists on a wide range of timescales:
48 from attempts to resolve geologically short-lived (kyr-scale) climate events from deep sea cores with low
49 sedimentation rates (e.g. Stap et al., 2010; Rodríguez-Sanz et al., 2017) to efforts to characterize tidal or
50 daily variability in accretionary carbonate archives (e.g. Warter and Müller, 2017; de Winter et al., 2020a).
51 What constitutes “high-resolution” is therefore largely dependent on the specifics of the climate archive.

52 Sample size limitations are especially important in paleoseasonality reconstructions. Reliable archives for
53 seasonality (e.g. corals, mollusks and speleothem records) are in high demand in the paleoclimate
54 community, because the seasonal cycle is one of the most important cycles in Earth’s climate and
55 seasonality reconstructions complement more common long-term (kyr to Myr) records of past climate
56 variability (e.g. Morgan and van Ommen, 1997; Tudhope et al., 2001; Steuber et al., 2005; Steffensen et
57 al., 2008; Denton et al., 2005; Huyghe et al., 2015; Vansteenberghe et al., 2019). A more detailed
58 understanding of climate dynamics at the human timescale is increasingly relevant for improving climate
59 projections (IPCC, 2013). Unfortunately, the growth and mineralization rates of archives that capture high-
60 resolution variability (only exceeding 10 mm/yr in rare exceptions, e.g. Johnson et al., 2019) limit the
61 number and size of samples that can be obtained at high temporal resolutions (e.g. Mosley-Thompson et
62 al., 1993; Passey and Cerling, 2002; Treble et al., 2003; Goodwin et al., 2003). In addition, accurate

63 positioning of samples within the seasonal cycle is challenging. In absence of fine-scale growth markings
64 (e.g. daily laminae in mollusk shells; e.g. Schöne et al., 2005; de Winter et al., 2020a), this dating problem
65 relies on modelling or interpolation of the growth of the archive, which introduces uncertainty on the age of
66 samples (e.g. Goodwin et al., 2009; Judd et al., 2018). These problems are exacerbated by the fact that
67 accurate methods for climate reconstructions may require comparatively large sample sizes, or rely on
68 uncertain assumptions. A case in point is the popular carbonate stable oxygen isotope temperature proxy
69 ($\delta^{18}\text{O}_c$) which relies on assumptions of the water composition ($\delta^{18}\text{O}_w$) that become progressively more
70 uncertain further back in geological history (e.g. Veizer and Prokoph, 2015). In contrast, the clumped
71 isotope proxy (Δ_{47}) does not rely on this assumption but requires larger amounts of sample (e.g. Müller et
72 al., 2017)

73 A promising technique for circumventing sample size limitations is to analyze larger numbers of small
74 aliquots from the same sample or from similar parts of the climate archive. These smaller aliquots typically
75 have poor precision but averaging multiple aliquots into one estimate while propagating the measurement
76 uncertainty leads to a more reliable estimate of the climate variable (Dattalo, 2008; Meckler et al., 2014;
77 Müller et al., 2017; Fernandez et al., 2017). This approach yields improved sampling flexibility since aliquots
78 can be combined in various ways after measurement. It also allows outlier detection at the level of individual
79 aliquots, thereby spreading the risk of instrumental failure and providing improved control on changes in
80 measurement conditions that may bias results.

81 Previous studies have applied several different methods for combining data from paleoclimate records to
82 reduce analytical noise or higher order variability, and extract variability with a specific frequency (e.g. a
83 specific orbital cycle or seasonality; e.g. Lisiecki and Raymo, 2005; Cramer et al., 2009). These data
84 reduction approaches can in general be categorized into **smoothing** techniques, in which a sliding window
85 or range of neighboring datapoints is used to smooth high resolution records (see e.g. Cramer et al., 2009)
86 or **binning** techniques, in which the record is divided into equal bins in the sampling direction (e.g. time,
87 depth or length in growth direction; e.g. Lisiecki and Raymo, 2004; Rodríguez-Sanz et al., 2017). In addition,
88 a third approach is proposed here based on **optimization** of sample size for dynamic binning of data along
89 the climate cycle using a moving window in the domain of the climate variable (as opposed to the sampling

90 domain) combined with a T-test routine (see section 2.1). All three approaches have advantages and
91 caveats.

92 In this study, we explore the (dis)advantages of these three data reduction approaches by testing their
93 reliability in resolving seasonal variability in sea surface temperature (SST) and water stable oxygen isotope
94 composition ($\delta^{18}\text{O}_w$), both highly sought-after variables in paleoclimate research. We compare
95 reconstructions of SST and $\delta^{18}\text{O}_w$ in real and virtual datasets from accretionary carbonate archives (e.g.
96 shells, corals and speleothems) using the clumped isotope thermometer (Δ_{47}) combined with stable oxygen
97 isotope ratios of the carbonate ($\delta^{18}\text{O}_c$).

98

99 2. Methods

100 2.1 Reconstruction approaches

101 Throughout the remainder of this work, the three approaches for combining data for reconstructions are
102 defined as follows (see also Fig. 1):

103 **Smoothing** refers to the reconstruction of SST and $\delta^{18}\text{O}_w$ based on **moving averages** of Δ_{47} and $\delta^{18}\text{O}_c$
104 records (Fig. 1B). For every dataset, the full possible range of moving window sizes (from 1 sample to the
105 full length of the record) for SST and $\delta^{18}\text{O}_w$ reconstructions was explored. The window size that resulted in
106 the most significant difference between maximum and minimum Δ_{47} values (based on a student's T-test)
107 was applied to reconstruct SST and $\delta^{18}\text{O}_w$ from Δ_{47} and $\delta^{18}\text{O}_c$ records. SST and $\delta^{18}\text{O}_w$ were calculated for
108 all case studies using a combination of empirical temperature relationships by Kim and O'Neil (1997; $\delta^{18}\text{O}_c$ -
109 $\delta^{18}\text{O}_w$ -temperature relationship) and Bernasconi et al. (2018; Δ_{47} -temperature relationship). To obtain $\delta^{18}\text{O}_w$
110 values, the $\delta^{18}\text{O}_c$ - $\delta^{18}\text{O}_w$ -temperature relationship (Kim and O'Neil, 1997) was solved for $\delta^{18}\text{O}_w$ using the
111 temperature reconstruction obtained from Δ_{47} measurements. Here and in other approaches, a typical
112 analytical uncertainty on measurements of Δ_{47} (one standard deviation of 0.04‰) and $\delta^{18}\text{O}_c$ (one standard
113 deviation of 0.05‰) was used to include uncertainty due to measurement precision. These analytical
114 uncertainties were chosen based on typical uncertainties reported for these measurements in the literature
115 (e.g. Schöne et al., 2005; Huyghe et al., 2015; Vansteenberghe et al., 2016) and long-term precision

116 uncertainties obtained by measuring in-house standards using the MAT253+ with Kiel IV setup in the
117 clumped isotope laboratory at Utrecht University (e.g. Kocken et al., 2019). The measurement uncertainty
118 was propagated through all calculations using a Monte Carlo simulation ($N = 1000$) in which Δ_{47} and $\delta^{18}\text{O}_c$
119 records were randomly sampled from a normal distribution with the virtual Δ_{47} and $\delta^{18}\text{O}_c$ values as means
120 and analytical uncertainties as standard deviations. Resulting SST and $\delta^{18}\text{O}_w$ values were grouped into
121 monthly time bins using the age model of the archive.

122 **Binning** refers to reconstructions of SST and $\delta^{18}\text{O}_w$ based on binning of Δ_{47} and $\delta^{18}\text{O}_c$ records into monthly
123 time bins (**Fig. 1C**). The Δ_{47} and $\delta^{18}\text{O}_c$ data from each case study were grouped into monthly time bins and
124 converted to SST and $\delta^{18}\text{O}_w$ using the Kim and O'Neil (1997) and Bernasconi et al. (2018) formulae. Here
125 too, Monte Carlo simulation ($N = 1000$) was applied to propagate measurement uncertainties onto monthly
126 SST and $\delta^{18}\text{O}_w$ reconstructions. Note that the prerequisite for this method is that the data is aligned using
127 a (floating) age model accurate enough to allow samples to be placed in the right bin. The age of virtual
128 samples in this study is known so this prerequisite poses no problems in this case. However, in the fossil
129 record this alignment might be less certain in the absence of accurate chronologies within the archive (e.g.
130 through daily growth increments in mollusk shells; e.g. Schöne et al., 2008; Huyghe et al., 2019; see 4.1.3).

131 **Optimization** refers to reconstructions of SST and $\delta^{18}\text{O}_w$ based on sample size optimization in Δ_{47} records
132 (**Fig. 1D**). In this approach aliquots of each dataset are ordered from warm (low $\delta^{18}\text{O}_c$) to cold (high $\delta^{18}\text{O}_c$)
133 data) samples, regardless of their position relative to the seasonal cycle. From this ordered dataset,
134 increasingly large samples of multiple aliquots (from 2 aliquots to half the length of the record) are taken
135 from both the warm ("summer") and the cold ("winter") side of the distribution. Summer and winter samples
136 were kept equal (symmetrical grouping) to reduce the number of possible sample size combinations and
137 allow for more efficient computation. However, asymmetrical grouping with differing sample sizes on the
138 summer and winter ends of the $\delta^{18}\text{O}_c$ -spectrum are possible (see 4.1.3 and 4.2.2). Sample sizes with
139 significant difference in Δ_{47} value between summer and winter groups ($p \leq 0.05$ based on a student's T-
140 test) were selected as optimal sample sizes. The moving window T-test in the proxy domain ensures that
141 an optimal compromise is reached between high precision and resolving differences between seasonal
142 extremes. For each successful sample size, SST and $\delta^{18}\text{O}_w$ values were calculated from Δ_{47} and $\delta^{18}\text{O}_c$ data

143 according to Kim and O'Neil (1997) and Bernasconi et al. (2018) formulae. The relationship between SST
144 and $\delta^{18}\text{O}_w$ obtained from these reconstructions was used to convert all Δ_{47} and $\delta^{18}\text{O}_c$ data to SST and
145 $\delta^{18}\text{O}_w$, which are then grouped into monthly SST and $\delta^{18}\text{O}_w$ reconstructions along the archive's age model.
146 Measurement uncertainties were propagated through the entire approach by Monte Carlo simulation (N =
147 1000).

148 For comparison, we also include reconstructions based solely on $\delta^{18}\text{O}_c$ measurements with an (often
149 inaccurate) assumption of a constant $\delta^{18}\text{O}_w$ (equal to the modern ocean value of 0‰ VSMOW), which form
150 the most common method for carbonate-based temperature reconstructions in paleoclimate research (see
151 e.g. Schöne et al., 2005; Westerhold et al., 2020; **Fig. 1A**; hereafter: **$\delta^{18}\text{O}$**). For these reconstructions, $\delta^{18}\text{O}_c$
152 records were grouped into monthly time bins with analytical uncertainties propagated using the Monte Carlo
153 approach (N = 1000) and were directly converted to SST using the Kim and O'Neil (1997) temperature
154 relationship.

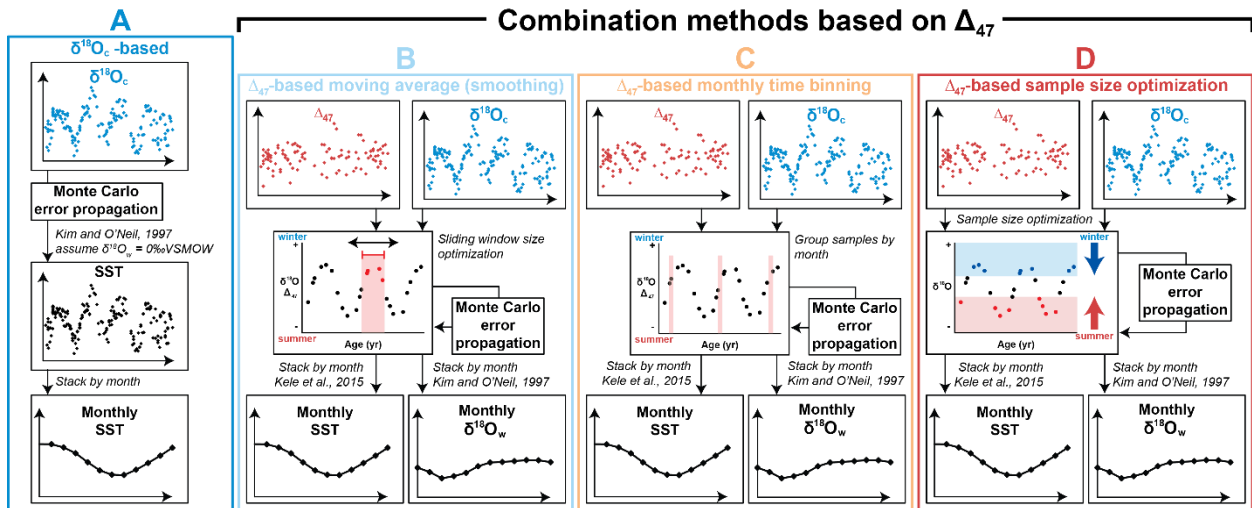
155 For each reconstruction, SST and $\delta^{18}\text{O}_w$ results were aggregated into monthly averages, medians, standard
156 deviations, and standard errors. Step by step documentation of calculations made for the three Δ_{47} -based
157 reconstruction approaches and the $\delta^{18}\text{O}_c$ reconstructions are given in **Supplimentary Data S7** and in the
158 complementary R package (de Winter, 2021a).

159 **2.2 Benchmarks for accuracy and precision**

160 Accuracy and precision of reconstructions were evaluated against official USGS definitions of climate
161 parameters (O'Donnell and Ignizio, 2012):

- 162 1. mean annual SST (MAT), defined as the average of all 12 monthly temperature reconstructions.
- 163 2. seasonal range in SST, defined as the temperature difference between warmest and coldest
164 month.
- 165 3. mean annual $\delta^{18}\text{O}_w$, defined as the average of all 12 monthly $\delta^{18}\text{O}_w$ reconstructions.
- 166 4. seasonal range in $\delta^{18}\text{O}_w$, defined as the $\delta^{18}\text{O}_w$ difference between most enriched (highest $\delta^{18}\text{O}_w$)
167 and most depleted (lowest $\delta^{18}\text{O}_w$) monthly reconstruction.

168 Accuracy was defined as the absolute offset of the reconstructed climate parameter from the “true” value.
 169 Precision was defined as the (relative) standard deviation of the reconstruction, as calculated from the
 170 variability within monthly time bins resulting from Monte Carlo error propagation (see 2.1). An overview of
 171 monthly SST and $\delta^{18}\text{O}_w$ reconstructions using the four approaches in all cases is given in S4. Raw data
 172 and figures of reconstructions of all cases using all sampling resolutions are compiled in S8.

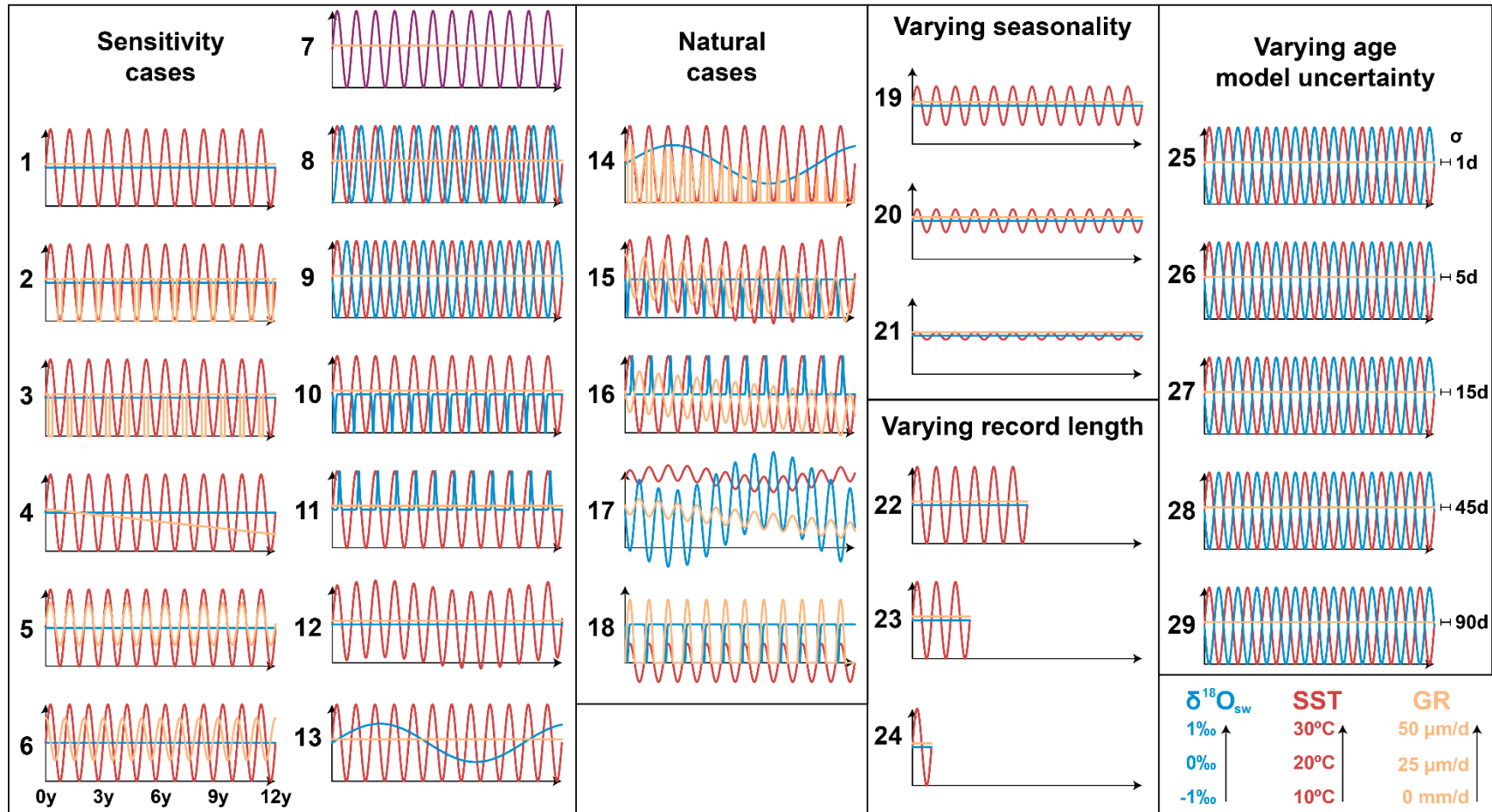


173
 174 **Figure 1:** Schematic overview of the four approaches for seasonality reconstructions: (A) $\delta^{18}\text{O}$ -based
 175 reconstructions, assuming constant $\delta^{18}\text{O}_w$. (B) Reconstructions based on **smoothing** $\delta^{18}\text{O}_c$ and Δ_{47} data
 176 using a moving average. (C) Reconstructions based on binning $\delta^{18}\text{O}_c$ and Δ_{47} data in monthly time bins.
 177 (D) Reconstructions based on **optimization** of the sample size for combining $\delta^{18}\text{O}_c$ and Δ_{47} data (see
 178 description in 2.1). Colored points represent virtual $\delta^{18}\text{O}_c$ (blue) and Δ_{47} (red) series in sampling domain.
 179 Black curves represent reconstructed monthly SST and $\delta^{18}\text{O}_w$ averages.

180
 181 **2.3 SST and $\delta^{18}\text{O}_w$ datasets**

182 The three reconstruction approaches were tested and compared based on three types of data. Firstly, a set
 183 of datasets based on fully artificial environmental SST and $\delta^{18}\text{O}_w$ data (case 1-29; see Fig. 2) converted to
 184 virtual Δ_{47} and $\delta^{18}\text{O}_c$ records. Secondly, data based on actual measurements of natural variability in SST
 185 and sea surface salinity (SSS; case 30-33) converted to virtual Δ_{47} and $\delta^{18}\text{O}_c$ records. Thirdly, measured
 186 proxy data from a real specimen of a Pacific oyster (*Crassostrea gigas*, syn. *Magallana gigas*) compared
 187 to measured environmental (SST and $\delta^{18}\text{O}_w$) data reported in Ullmann et al. (2010).

Virtual cases



188

189 **Figure 2:** Overview of time series of all virtual test cases. Colored curves represent time series of SST (red), $\delta^{18}\text{O}_w$ (blue),
 190 abbreviated as “GR”). Horizontal axes in all plots are 12 years long (see legend below case 6). Vertical axis of all plots has the same scale (SST:
 191 10 to 30°C; $\delta^{18}\text{O}_w$: -1 to +1‰; Growth rate: 0–50 $\mu\text{m}/\text{day}$; see legend in bottom right corner). Horizontal error bars and labels on the right side of
 192 cases 25-29 represent standard errors introduced on the age model (bars not to scale). The $\delta^{18}\text{O}_c$ and Δ_{47} records resulting from these virtual
 193 datasets are provided in **S6** (see also **Fig. 3** for natural examples).

Sensitivity cases		Natural cases	Varying seasonality	Varying age model uncertainty		
1. Control	7. $\delta^{18}\text{O}_w$ seasonality in phase with SST	14. Full marine case with ontogenetic GR trend	19. Control case with reduced SST amplitude ($\sim 5^\circ\text{C}$)	25. Case 9 with ± 1 day age model uncertainty		
	8. $\delta^{18}\text{O}_w$ seasonality in antiphase with SST		20. Control case with reduced SST amplitude ($\sim 3^\circ\text{C}$)			
	2. Growth stops $< 12^\circ\text{C}$		9. $\delta^{18}\text{O}_w$ seasonality lags SST by $\frac{1}{4}$ year		21. Control case with reduced SST amplitude ($\sim 1^\circ\text{C}$)	26. Case 9 with ± 5 days age model uncertainty
	3. Growth stops $> 28^\circ\text{C}$		10. Negative $\delta^{18}\text{O}_w$ in spring		Varying record length	
	4. Linear decrease in GR		11. Positive $\delta^{18}\text{O}_w$ in summer		22. Control case shortened to 6 yr	27. Case 9 with ± 15 days age model uncertainty
	5. GR seasonality in phase with SST		12. Multi-annual (5 yr) SST cycle		23. Control case shortened to 3 yr	28. Case 9 with ± 45 days age model uncertainty
6. GR seasonality lags SST by $\frac{1}{4}$ year	13. Multi-annual (5 yr) $\delta^{18}\text{O}_w$ cycle	15. Coastal case with spring $\delta^{18}\text{O}_w$ decrease and decreasing GR trend	29. Case 9 with ± 90 days age model uncertainty			
		16. Lagoonal case with summer $\delta^{18}\text{O}_w$ increase	24. Control case shortened to 1 yr			
		17. Tropical monsoon case with confined SST seasonality and strong multi-annual SST cycle				
		18. Worst-case scenario with growth limited to summer half of the year				

194 **Table 1:** Overview of virtual cases 1-29 used to test the reconstruction methods. Case descriptions are
195 abbreviated. Details on the SST, growth rate and $\delta^{18}\text{O}_w$ included in each case are described in detail in **S1**.
196 SST, growth rate and $\delta^{18}\text{O}_w$ records of all cases are shown in **Fig. 2**. “GR” = growth rate.

197

198 2.3.1 Cases 1-29: Virtual environmental data, virtual proxy data

199 Virtual SST and $\delta^{18}\text{O}_w$ time series were artificially constructed to test the effect of various SST and $\delta^{18}\text{O}_w$
200 scenarios on the effectivity of the reconstruction methods. The default test case (case 1) contained an ideal,
201 12-year sinusoidal SST curve with a period of 1 year (seasonality), a mean value of 20°C and a seasonal
202 amplitude of 10°C , a constant $\delta^{18}\text{O}_w$ value of 0‰ and a constant growth rate of 10 mm/yr. Other cases
203 contain various deviations from this ideal case (see also **Fig. 2**, **Table 1** and **S1**):

- 204 • Linear and/or seasonal changes in growth rate, including growth stops (cases 2-6, 14-18)

- 205 • Seasonal and/or multi-annual changes in $\delta^{18}\text{O}_w$ (cases 7-11, 13-18)
- 206 • Multi-annual trends in SST superimposed on the seasonality (cases 12, 15 and 17)
- 207 • Variations in the seasonal SST amplitude (cases 19-21)
- 208 • Change in the total length of the time series (cases 22-24).
- 209 • Variation in uncertainty on the age of each virtual datapoint (cases 25-29)

210 Comparison of the virtual time series (case 1-29; **Fig. 2**) with the natural variability (case 30-33; **Fig. 3**)
211 shows that the virtual cases are not realistic approximations of natural variability in SST and $\delta^{18}\text{O}_w$. Natural
212 SST and $\delta^{18}\text{O}_w$ variability are not limited to the seasonal or multi-annual scale but contain a fair amount of
213 higher order (daily to weekly scale) variability. To simulate this natural variability, we extracted the seasonal
214 component of SST and $\delta^{18}\text{O}_w$ variability from our highest resolution record of measured natural SST and
215 SSS data (case 30: data from Texel, the Netherlands, see **2.3.2** and **Fig. 3**). The standard deviation of
216 residual variability of this data after subtraction of the seasonal cycle was used to add random high-
217 frequency noise to the SST and $\delta^{18}\text{O}_w$ variability in virtual cases. Note that while sub-annual environmental
218 variability can be approximated by Gaussian noise (Wilkinson and Ivany, 2002), this representation is an
219 oversimplification of reality. In the case of our Texel data, the SST and SSS residuals are not normally
220 distributed (Kolmogorov-Smirnov test: $D = 0.010$; $p = 7.2 \cdot 10^{-14}$ and $D = 0.039$; $p < 2.2 \cdot 10^{-16}$ for SST and
221 SSS residuals respectively; see **S2-4**). SST and $\delta^{18}\text{O}_w$ data from cases 1-29 was converted to the sampling
222 domain and subsampled at a range of sampling resolutions following the same procedure applied to cases
223 30-33 (see **2.3.2**).

224

225 *2.3.2 Cases 30-33: Measured environmental data, virtual proxy data*

226 Four test cases were based on time series of real measured SST and SSS data from four different locations,
227 selected to capture a variety of environments with different SST and SSS variability (see **Fig. 3**):

- 228 1. Tidal flats of the Wadden Sea near Texel, the Netherlands (case 30)
- 229 2. Great Barrier Reef in Australia (case 31)
- 230 3. Gulf of Aqaba between Egypt and Saudi Arabia (case 32)

231 4. Northern Atlantic Ocean east of Iceland (case 33).

232 Daily measurements of SST and SSS for case 31-33 were obtained from worldwide open-access datasets
233 of the National Oceanic and Atmospheric Administration (NOAA, 2020) and European Space Agency (ESA,
234 2020) respectively. Hourly SST and SSS measured *in situ* in the Wadden Sea (case 30) were obtained
235 from the Dutch Institute for Sea Research (NIOZ, Texel, the Netherlands). Since direct, *in situ*
236 measurements of $\delta^{18}\text{O}_w$ variability at a high temporal resolution were not available, $\delta^{18}\text{O}_w$ was estimated
237 from more widely available SSS data using a mass balance (equation 1 and 2; following e.g. Ullmann et
238 al., 2010):

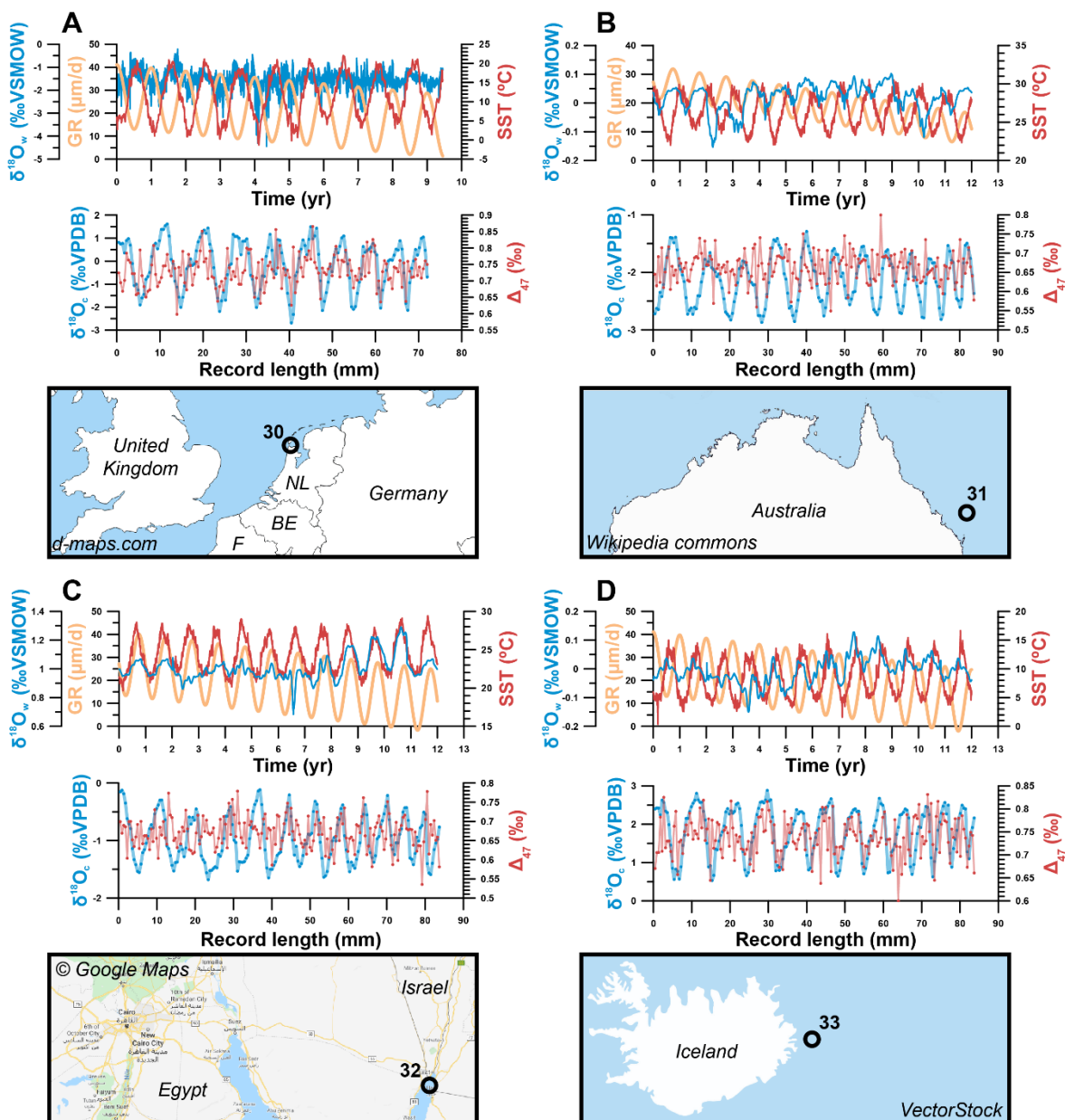
$$239 \delta^{18}\text{O}_{sw} = \delta^{18}\text{O}_{w,freshwater} * f + \delta^{18}\text{O}_{w,ocean} * (1 - f) \quad (1)$$

$$240 f = \frac{SSS_{sample} - SSS_{ocean}}{SSS_{freshwater} - SSS_{ocean}} \quad (2)$$

241 Here, we assume salinity (SSS_{sample}) results from a mixture of a fraction (f) isotopically light and low-salinity
242 ($\delta^{18}\text{O}_{w,freshwater} = -8\text{‰}$; $SSS_{freshwater} = 0$) freshwater and a fraction ($1-f$) ocean water ($\delta^{18}\text{O}_{w,ocean} = 0\text{‰}$;
243 $SSS_{ocean} = 35$), with negative amounts of freshwater contribution ($f < 0$) representing net evaporation
244 ($SSS_{sample} > SSS_{ocean}$). The value for $\delta^{18}\text{O}_{w,freshwater}$ was based on the $\delta^{18}\text{O}_w$ of rain in the Netherlands (-8‰ ;
245 Mook, 1970; Bowen, 2020). Applying this mass balance on the SSS record of the Wadden Sea tidal flats
246 (case 30) results in $\delta^{18}\text{O}_w$ values and a SSS- $\delta^{18}\text{O}_w$ relationship in agreement with measurements in this
247 region (Harwood et al., 2008). SST and $\delta^{18}\text{O}_w$ time series for all cases are given in **Supplementary Data**
248 **S4** and natural cases are plotted in **Fig. 3**.

249 For all virtual proxy datasets (cases 1-33), records of SST and $\delta^{18}\text{O}_w$ were converted to the sampling
250 domain (along the length of the record) by defining a virtual growth rate in the sampling direction. Adding
251 this growth rate as a variable allowed us to test the sensitivity of approaches to changes in the extension
252 rate of the archive, including hiatuses (growth rate = 0). This is important, because fluctuations in linear
253 extension rate and periods in which no mineralization occurs (hiatuses or growth cessations) are common
254 in all climate archives (e.g. Treble et al., 2003; Ivany, 2012). After conversion to the sampling domain, virtual
255 aliquots were subsampled at equal distance from the SST and $\delta^{18}\text{O}_w$ series of all cases using six sampling
256 intervals: 0.1 mm, 0.2 mm, 0.45 mm, 0.75 mm, 1.55 mm and 3.25 mm. The four largest sampling intervals

257 were chosen such that the standard growth rate (10 mm/yr) was not an integer multiple of the sampling
 258 interval (e.g. 0.45 mm instead of 0.5 mm, and 3.25 mm instead of 3 mm). This decision prevents sampling
 259 the same parts of the seasonal cycle (e.g. same months) every year, which biases both the mean value
 260 and the precision of monthly SST and $\delta^{18}\text{O}_w$ reconstructions. This bias towards certain parts of the seasonal
 261 cycle is much stronger at low sample sizes (large sampling intervals) and is illustrated in the
 262 **Supplementary Figure S2.**



263

264 **Figure 3:** Overview of the four cases of virtual data based on natural SST and SSS measurements explored
265 in this study. (A) Case 30: Tidal flats on the Wadden Sea, Texel, the Netherlands. (B) Case 31 Great Barrier
266 Reef, Australia). (C) Case 32: Gulf of Aqaba between Egypt and Saudi Arabia. (D) Case 33: Atlantic Ocean
267 east of Iceland. For all cases, graphs on top show environmental data, with SST plotted in red, $\delta^{18}\text{O}_w$ in
268 blue and growth rate (abbreviated as "GR") in orange (as in **Fig. 2**). The graph below shows virtual $\delta^{18}\text{O}_c$
269 (blue) and Δ_{47} (red) records created from these data series using a sampling interval of 0.45 mm and
270 including analytical noise (see **3.3**). Note that the scale of vertical axes varies between plots.

271

272 2.3.3 Modern oyster: Measured environmental data, measured proxy data

273 Environmental SST and $\delta^{18}\text{O}_w$ data from the List Basin in Denmark (54°59.25N, 8°23.51E), where the
274 modern oyster specimen lived, were obtained from local *in situ* measurements of SST and SSS described
275 in Ullmann et al. (2010). Since direct, *in situ* measurements of $\delta^{18}\text{O}_w$ variability at a high temporal resolution
276 were not available, $\delta^{18}\text{O}_w$ was estimated from more widely available SSS data using the mass balance
277 described in **2.3.2**. The value for $\delta^{18}\text{O}_{w,\text{freshwater}}$ was based on the discharge weighted average $\delta^{18}\text{O}_w$ of
278 water in the nearby Elbe and Weser rivers (see Ullmann et al., 2010). All $\delta^{18}\text{O}_w$ values throughout the text
279 are with reference to the VSMOW scale. Contrary to the virtual datasets (cases 1-33; see **2.3.1** and **2.3.2**),
280 the Ullmann et al. (2010) data was already available in the sampling domain, hence no subsampling was
281 required.

282

283 **2.4 Conversion to $\delta^{18}\text{O}_c$ and Δ_{47} data**

284 After subsampling, SST and $\delta^{18}\text{O}_w$ series (cases 1-33) were converted to $\delta^{18}\text{O}_c$ and Δ_{47} using a carbonate
285 model based on empirical relationships between Δ_{47} and $\delta^{18}\text{O}_c$ with SST and $\delta^{18}\text{O}_w$ (equation 3 and 4; Kim
286 and O'Neil, 1997; Kele et al., 2015; Bernasconi et al., 2018) and the conversion of $\delta^{18}\text{O}$ values from
287 VSMOW to VPDB scale (equation 5; Brand et al., 2014).

288
$$\Delta_{47} = \frac{0.0449 \cdot 10^6}{(SST+273.15)^2} + 0.167 \quad (3)$$

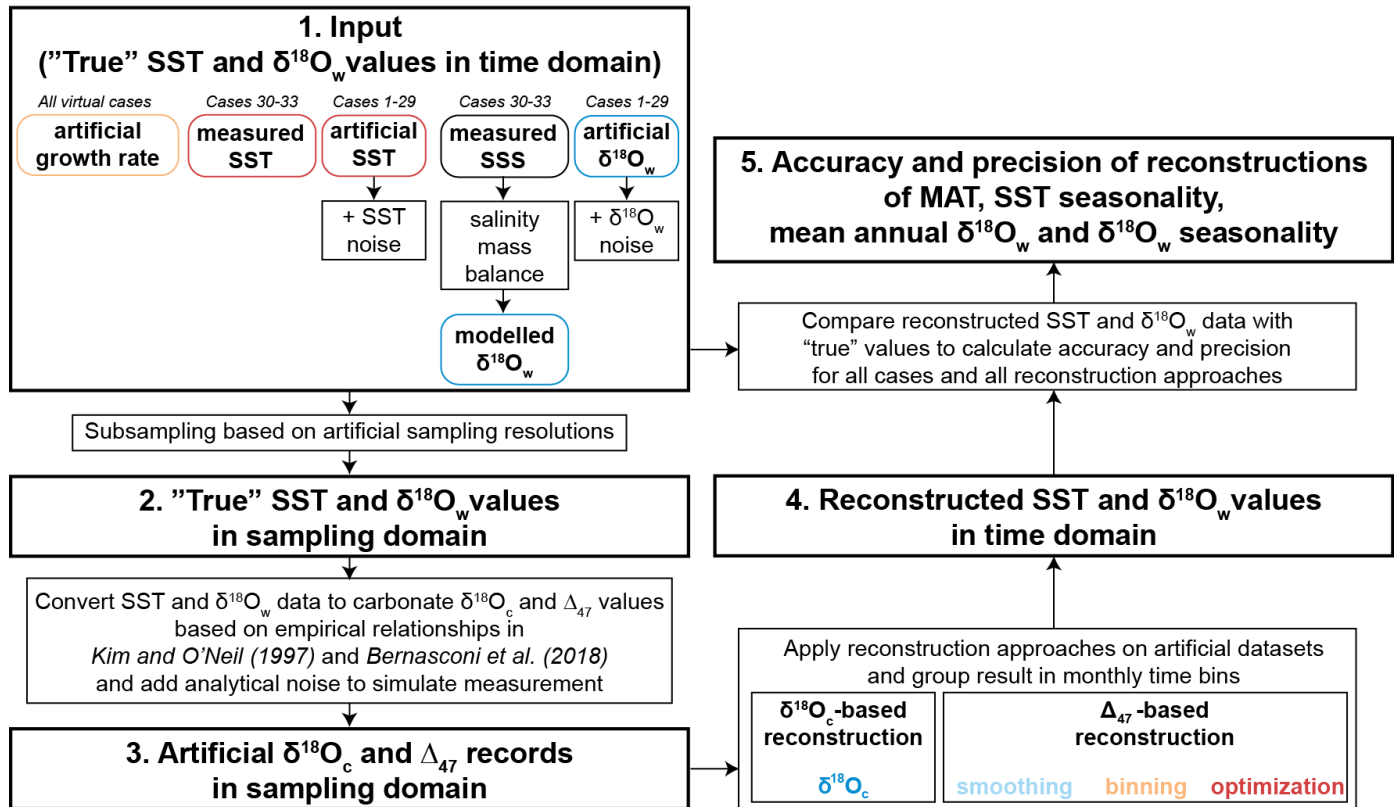
289
$$1000 * \ln \frac{\left(\frac{^{18}\text{O}}{^{16}\text{O}}\right)_{\text{CaCO}_3}}{\left(\frac{^{18}\text{O}}{^{16}\text{O}}\right)_{\text{H}_2\text{O}}} = 18.03 * \left(\frac{10^3}{(SST+273.15)}\right) - 32.42 \quad (4)$$

290
$$\delta^{18}\text{O}_{VPDB} = 0.97002 * \delta^{18}\text{O}_{VSMOW} - 29.98 \quad (5)$$

291 For the modern oyster data (Ullmann et al., 2010; see **2.3.3**), only the Δ_{47} data needed to be created
292 because $\delta^{18}\text{O}_c$ was directly measured. As a result, each case study yielded records of Δ_{47} and $\delta^{18}\text{O}_c$ in the
293 sampling domain and corresponding “true” SST and $\delta^{18}\text{O}_w$ records in the time domain, allowing assessment
294 of the reliability of the reconstruction approaches in different scenarios (**Fig. 4**). The result of applying these
295 steps is illustrated on case 31 (Great Barrier reef data, **Fig. 5**). All calculations for creating Δ_{47} and $\delta^{18}\text{O}_c$
296 series in sampling domain were carried out using the open-source computational software R (R core team,
297 2013), and scripts for these calculations are given in **Supplementary Data S7** and compiled in the
298 documented R package “seasonalclumped” (de Winter, 2021a). All Δ_{47} and $\delta^{18}\text{O}_c$ datasets are provided in
299 **Supplementary Data S6**.

300

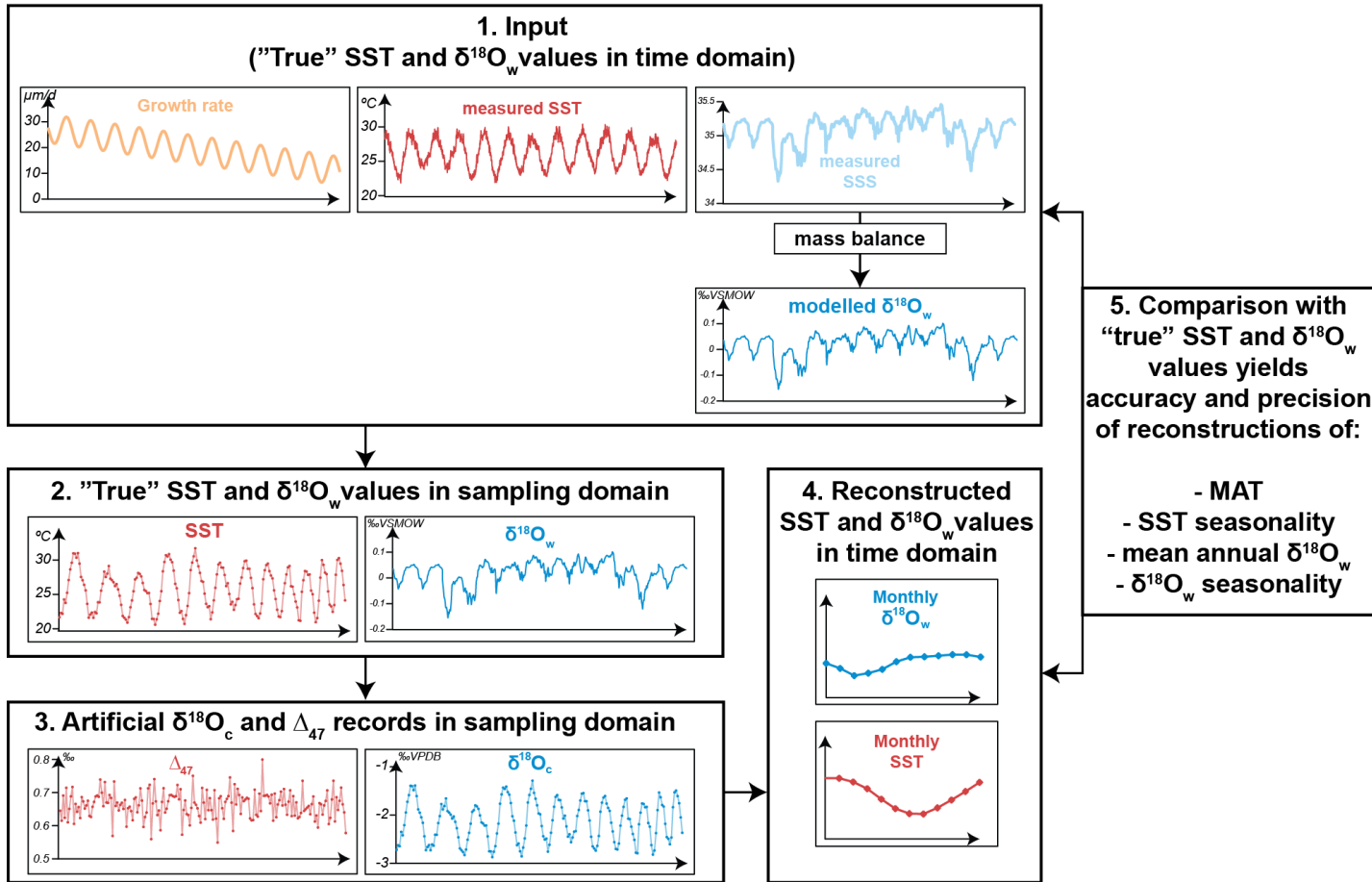
Workflow for creating virtual datasets and testing reconstruction approaches



301

302 **Figure 4:** Flow diagram showing the steps taken to create virtual data (Δ_{47} and $\delta^{18}O_c$; cases 1-33) and
 303 compare results of SST and $\delta^{18}O_w$ reconstructions with the actual SST and $\delta^{18}O_w$ data the record was
 304 based on (counterclockwise direction). Steps 1-3 outline the procedure for creating virtual Δ_{47} and $\delta^{18}O_c$
 305 datasets (see sections 2.3 and 2.4), step 4 shows the application of the different reconstruction methods
 306 on this virtual data (see Fig. 2 for details) and step 5 illustrates how the reconstructions are compared with
 307 the original ("true") SST and $\delta^{18}O_w$ data to calculate accuracy and precision of the reconstruction
 308 approaches. Note that step 1 is different for cases 1-29 (based on fully artificial SST and $\delta^{18}O_w$ records;
 309 2.3.1) than for cases 30-33 (SST and $\delta^{18}O_w$ records based on real SST and SSS data; see 2.3.2).

Workflow for creating virtual datasets and testing reconstruction approaches:
 Example for case 31 (Great Barrier Reef satellite data)



310

311 **Figure 5:** An example of the steps highlighted in Fig. 4 using case 31 (Great Barrier Reef data) to illustrate
 312 the data processing steps. Virtual data plots include normally distributed measurement uncertainty on Δ_{47}
 313 and $\delta^{18}\text{O}_c$

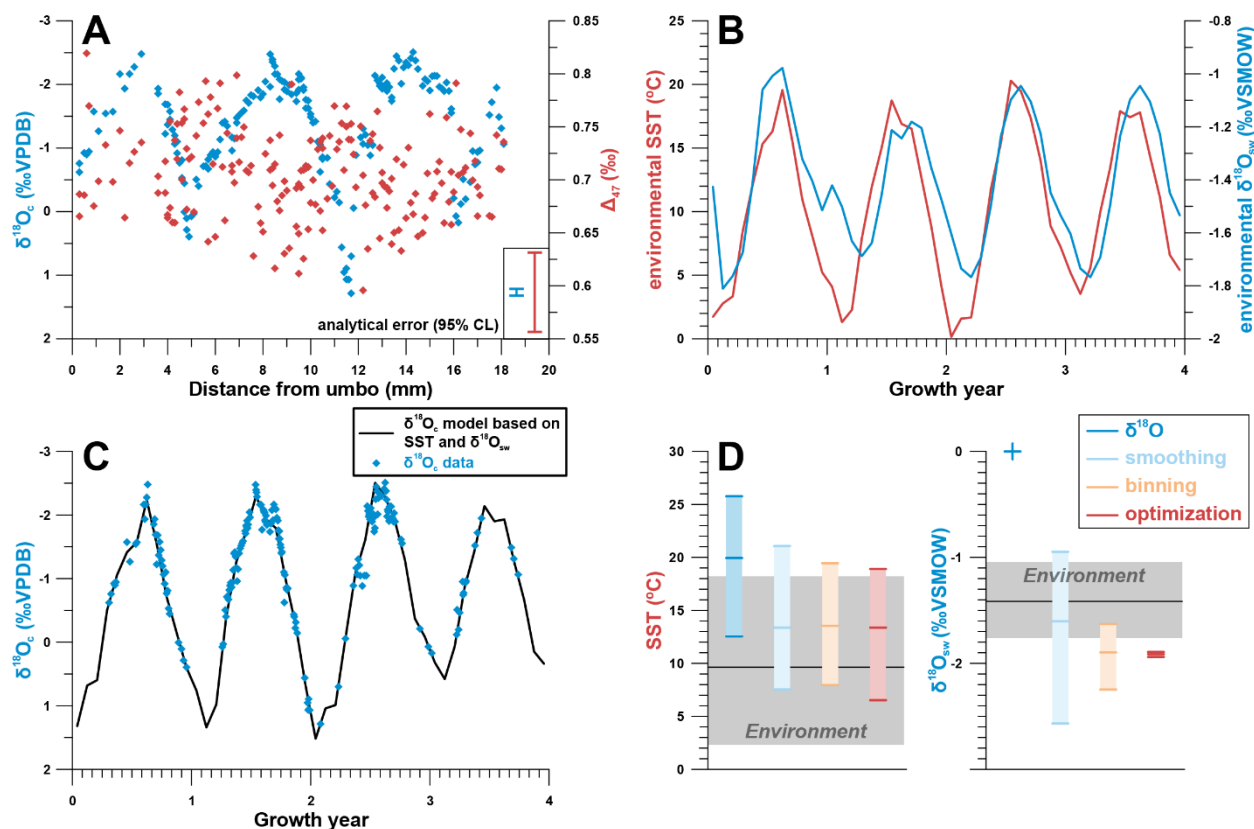
314

315 3. Results

316 3.1 Real example

317 Measured ($\delta^{18}\text{O}_c$) and simulated (Δ_{47}) data from the Pacific oyster from the Danish List Basin yielded
318 estimates of SST and $\delta^{18}\text{O}_w$ seasonality using all reconstruction approaches (**Fig. 6**). While a model of shell
319 $\delta^{18}\text{O}_c$ based on SST and SSS data closely approximates the measured $\delta^{18}\text{O}_c$ record (**Fig. 6C**), basing SST
320 reconstructions solely on $\delta^{18}\text{O}_c$ data without any *a priori* knowledge of $\delta^{18}\text{O}_w$ variability (assuming constant
321 $\delta^{18}\text{O}_w$ equal to the global marine value) leads to high inaccuracy in mean annual SST (**Fig. 6D**). Note that,
322 in absence of significant $\delta^{18}\text{O}_w$ seasonality (as in this case study), seasonal temperature range
323 reconstructions from $\delta^{18}\text{O}_c$ measurements can be very accurate. However, assuming constant $\delta^{18}\text{O}_w$ year-
324 round may introduce considerable bias (see **Fig. 7 and 8**). The in-phase relationship between SST and
325 SSS (**Fig. 6B**) slightly dampens the seasonal $\delta^{18}\text{O}_c$ cycle, causing underestimation of temperature
326 seasonality, while a negative mean annual $\delta^{18}\text{O}_w$ value in the List Basin biases SST reconstructions towards
327 higher temperatures. In terms of SST reconstructions, the **smoothing**, **binning** and **optimization**
328 approaches based on Δ_{47} and $\delta^{18}\text{O}_c$ data yield more accurate reconstructions, albeit with a reduced
329 seasonality and a bias towards the summer season. The latter is a result of severely reduced growth rates
330 in the winter season, which was therefore undersampled (see **Fig. 6A and 6C**). Approaches including Δ_{47}
331 data also yield far more accurate $\delta^{18}\text{O}_w$ estimates than the **$\delta^{18}\text{O}$** approach. However, the accuracy of $\delta^{18}\text{O}_w$
332 seasonality and mean annual $\delta^{18}\text{O}_w$ estimates is low in these approaches too, largely because of the limited
333 sampling resolution, especially in winter. The **optimization** approach suffers from the strong in-phase
334 relationship between SST and SSS, which obscures the difference between the $\delta^{18}\text{O}_w$ effect and the
335 temperature effect on shell carbonate. Yet, disentangling SST from $\delta^{18}\text{O}_w$ seasonality is central to the
336 success of the approach (see **3.4**). **Fig. 6D** does not show the precision on SST and $\delta^{18}\text{O}_w$ estimates, which
337 is much lower for the **smoothing** approach than for the **binning** and **optimization** approaches due to the
338 limited data in the winter seasons (see **Supplementary Data S6**). These results show that several
339 properties of carbonate archives, such as growth rate variability, phase relationships between SST and
340 $\delta^{18}\text{O}_w$ seasonality and sampling resolution, can impact the reliability of paleoseasonality reconstructions.

341 The virtual and real data cases in this study were tailored to test the effects of these archive properties
 342 more thoroughly.

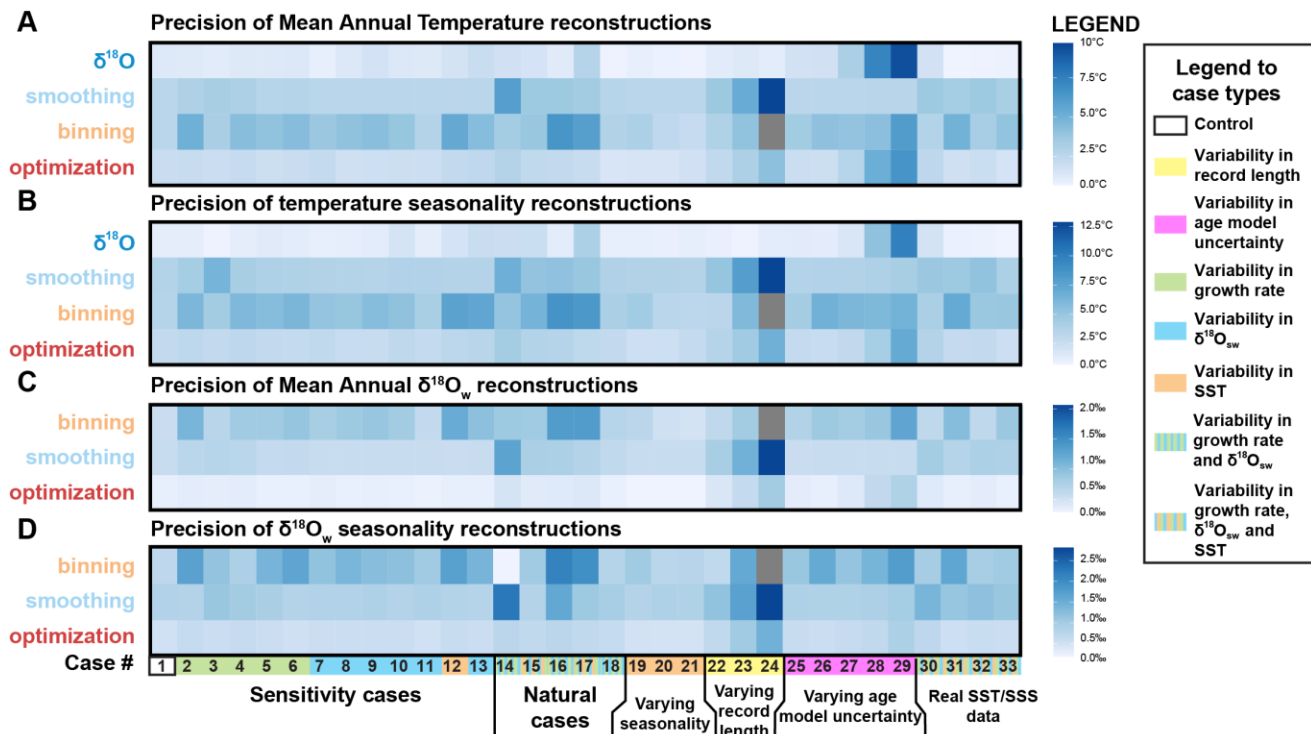


343
 344 **Figure 6:** (A) Plot of $\delta^{18}O_c$ and (virtual) Δ_{47} data from a modern Pacific oyster (*Crassostrea gigas*; see
 345 Ullmann et al., 2010). (B) shows SST and $\delta^{18}O_w$ data from the List Basin (Denmark) in which the oyster
 346 grew. (C) shows the fit between $\delta^{18}O_c$ data and modelled $\delta^{18}O_c$ calculated from SST and $\delta^{18}O_w$ on which
 347 the shell age model was based. (D) Shows a summary of the results of different approaches for
 348 reconstructing SST and $\delta^{18}O_w$ from the $\delta^{18}O_c$ and Δ_{47} data. The vertical colored bars show the reconstructed
 349 seasonal variability using all methods with ticks indicating warmest month, coldest month, and annual
 350 mean. The grey horizontal bars show the actual seasonal variability in the environment. Precision standard
 351 deviation on monthly reconstructions are not shown but are given in S4.

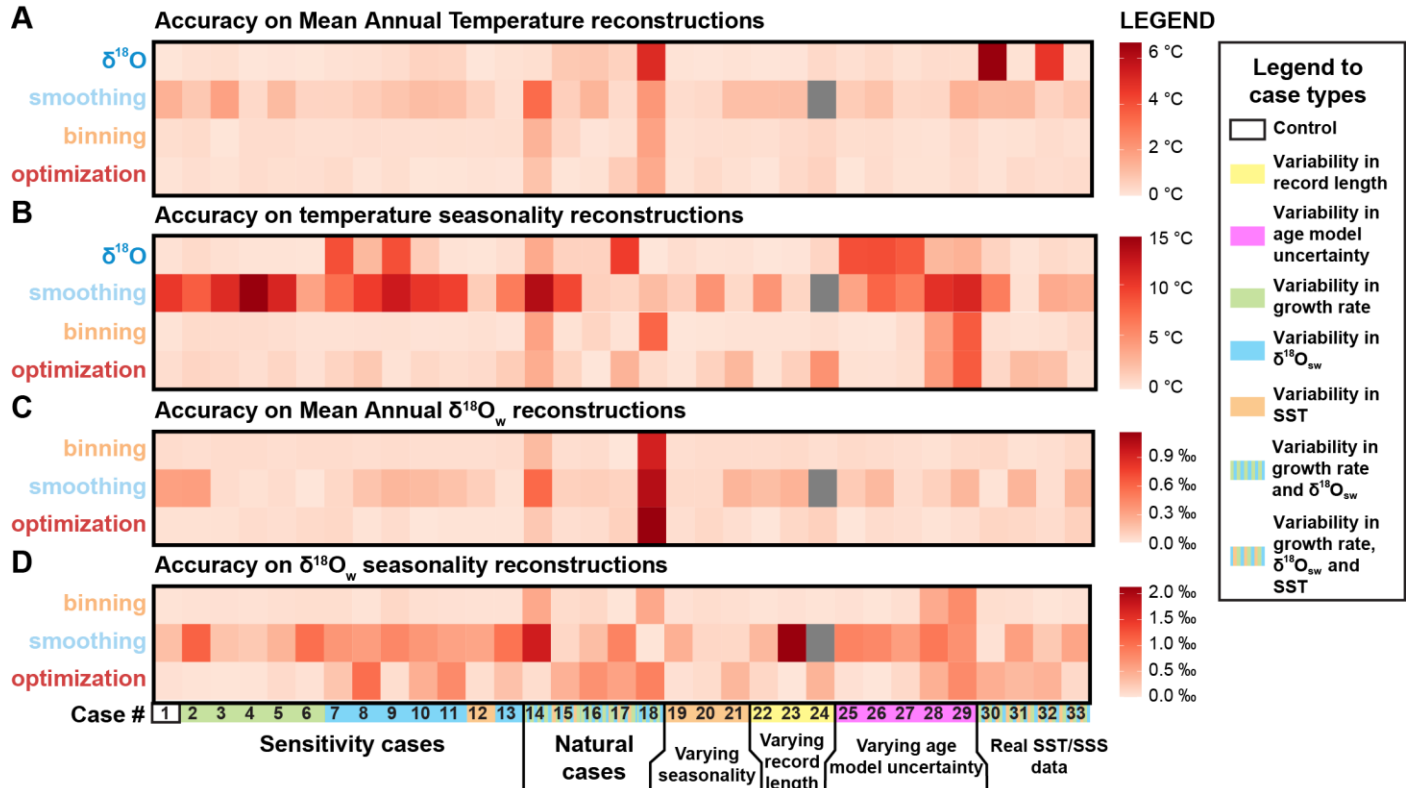
352
 353 **3.2 Case-specific results**
 354 A case-by-case breakdown of the precision (Fig. 7) and accuracy (Fig. 8) of reconstructions using the four
 355 approaches shows that reliability of reconstructions varies significantly between approaches and is highly
 356 case-specific. In general, precision is highest in $\delta^{18}O$ reconstructions, followed by **optimization** and
 357 **binning**, with **smoothing** generally yielding the worst precision. Average standard deviations of the
 358 underperforming methods (**binning** and **smoothing**) are up to 2-3 times larger than those of $\delta^{18}O$ (e.g.

359 respectively 3.9°C and 3.5°C vs. 1.3°C for $\delta^{18}\text{O}$ MAT reconstructions; see also **Supplementary**
360 **Information**). It is worth noting that precision on $\delta^{18}\text{O}$ -based estimates is mainly driven by measurement
361 precision (which is better for $\delta^{18}\text{O}_c$ than for Δ_{47} measurements, see section 4.1.1). Δ_{47} -based reconstructions
362 lose precision due to the higher measurement error on Δ_{47} measurements and the method used for
363 combining measurements for seasonality reconstructions. On a case-by-case basis, the hierarchy of
364 approaches can vary, especially if strong variability in growth rate is introduced, such as in case 14, where
365 the size of hiatuses in the record increases progressively, or in case 18, in which half of the year is missing
366 due to growth hiatuses (see **Table 1**, **Supplementary Data S1** and **S4**). Of the Δ_{47} -based methods
367 (**smoothing**, **binning** and **optimization**), **optimization** is rarely outcompeted in terms of precision in both
368 SST and $\delta^{18}\text{O}_w$ reconstructions.

369 The comparison based on precision alone is misleading, as the most precise approach ($\delta^{18}\text{O}$) runs the risk
370 of being highly inaccurate (offsets exceeding 4°C on some MAT reconstructions; see **Fig. 8A**), especially
371 in cases based on natural SST and SSS measurements (case 30-33). The **smoothing** approach also often
372 yields highly inaccurate results, especially in cases with substantial variability in $\delta^{18}\text{O}_w$ (e.g. case 9-11; **Fig.**
373 **8**). Accuracy of **optimization** and **binning** outcompete the other methods in most circumstances. **Binning**
374 outperforms **optimization** in reconstructions of $\delta^{18}\text{O}_w$ seasonality, making it overall the most accurate
375 approach. Interestingly, **optimization** is less accurate specifically in cases with sharp changes in growth
376 rate in summer (e.g. cases 11, 14, 16 and 17), while **binning** performs better in these cases.
377 Reconstructions of mean annual SST and $\delta^{18}\text{O}_w$ in case 18 are especially inaccurate regardless of which
378 method is applied. This extreme case with growth only during one half of the year combined with seasonal
379 fluctuations in both SST and $\delta^{18}\text{O}_w$ presents a worst-case scenario for seasonality reconstructions leading
380 to strong biases in mean annual temperature reconstructions. In situations like case 18, the **optimization**
381 approach is most accurate in MAT and SST seasonality reconstructions, but $\delta^{18}\text{O}_w$ is more accurately
382 reconstructed using the **binning** approach. Finally, it is worth noting that in natural situations (**Fig. 3**),
383 variability in SST almost invariably has a larger influence on $\delta^{18}\text{O}_c$ and Δ_{47} records than $\delta^{18}\text{O}_w$, such that
384 fluctuations in $\delta^{18}\text{O}_c$ records closely follow the SST seasonality even in cases with relatively large $\delta^{18}\text{O}_w$
385 variability (e.g. case 30). Chronologies based on these $\delta^{18}\text{O}_c$ fluctuations are therefore generally accurate.



387 **Figure 7:** Overview of precision (propagated standard deviation of variability within reconstructions, see
 388 **2.2**) of reconstructions of mean annual temperature (**A**), seasonal temperature range (**B**), mean annual
 389 $\delta^{18}\text{O}_w$ (**C**) and seasonal range in $\delta^{18}\text{O}_w$ (**D**), with higher values (darker colors) indicating lower precision
 390 (more variability between reconstructions) based on average sampling resolution (sampling interval of 0.45
 391 mm). The different cases on the horizontal axis are color coded by their difference from the control case
 392 (case 1; see legend on the right-hand side). Grey boxes indicate cases for which reconstructions were not
 393 successful. All data on precision (standard deviation values) is provided in **Supplementary Data S4**.

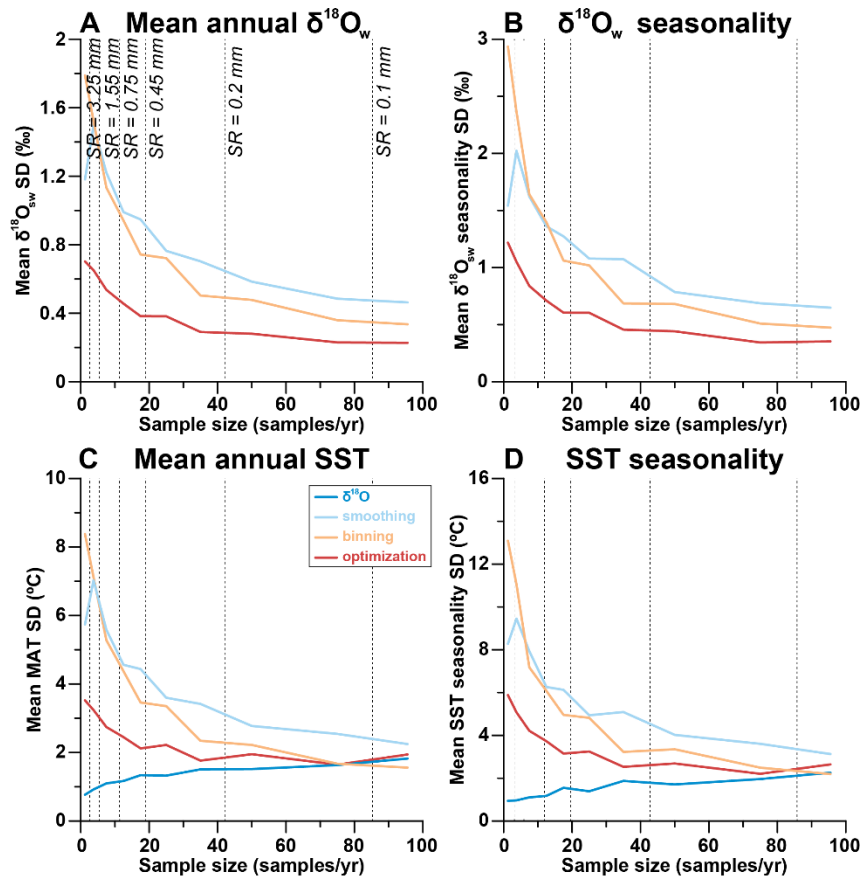


394

395 **Figure 8:** Overview of accuracy (absolute offset from “true” values) of reconstructions of mean annual
 396 temperature (A), seasonal temperature range (B), mean annual $\delta^{18}\text{O}_w$ (C) and seasonal range in $\delta^{18}\text{O}_w$ (D),
 397 with higher values (darker colors) indicating lower accuracy (higher offsets) based on average sampling
 398 resolution (sampling interval of 0.45 mm). The different cases on the horizontal axis are color coded by
 399 their difference from the control case (case 1; see legend on the right-hand side). Grey boxes indicate
 400 cases for which reconstructions were not successful. All data on accuracy (difference between
 401 reconstructed and “true” values) is provided in **Supplementary Data S4**.

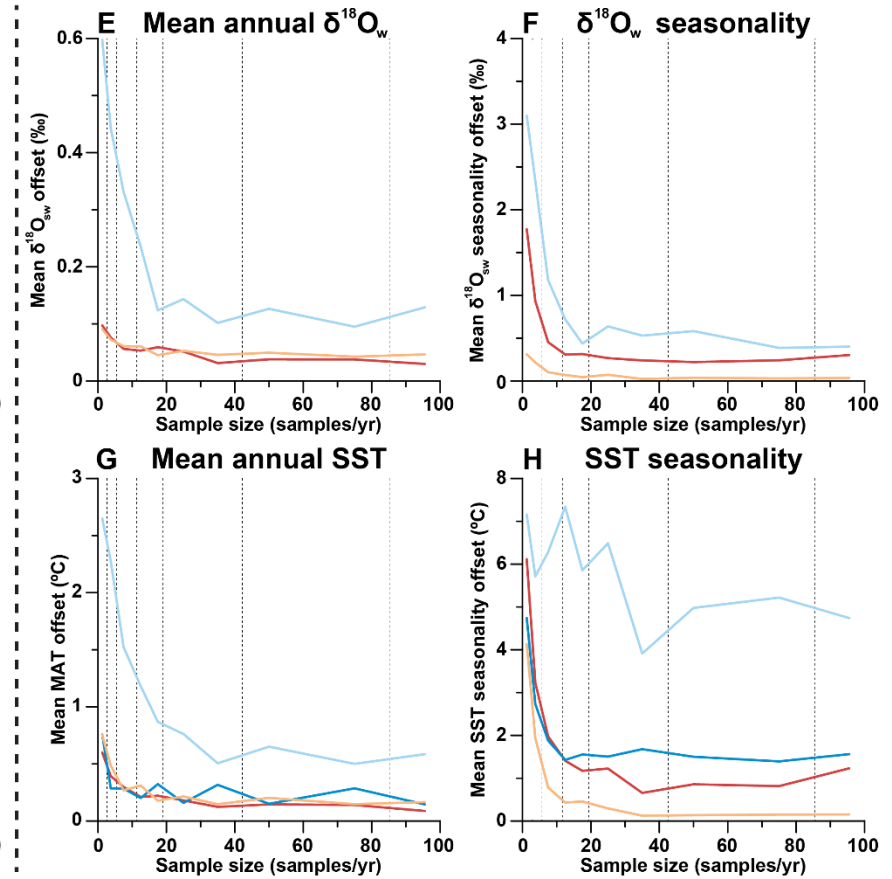
402

Precision



403

Accuracy

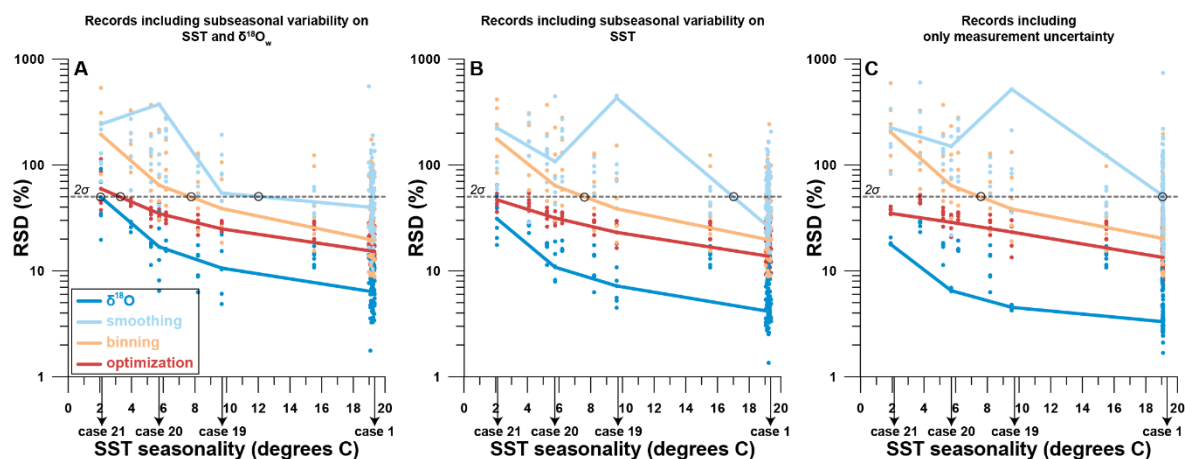


404 **Figure 9:** Effect of sampling resolution (in samples per year, see **S5**) on the precision (one standard deviation) of results of reconstructions of mean
 405 annual $\delta^{18}\text{O}_w$ (**A**), seasonal range in $\delta^{18}\text{O}_w$ (**B**), mean annual SST (**C**) and seasonal range in SST (**D**). Effect on the accuracy (absolute offset from
 406 actual value) of results of reconstructions of mean annual $\delta^{18}\text{O}_w$ (**E**) and seasonal range in $\delta^{18}\text{O}_w$ (**F**), mean annual SST (**G**) and seasonal range in
 407 SST (**H**). Color coding follows the scheme in **Fig. 1** and **Fig. 4**.

408 3.3 Effect of sampling resolution

409 As expected, increasing the temporal sampling resolution (i.e. number of samples per year) almost
 410 invariably increases the precision and accuracy (**Fig. 9**) of reconstructions using all methods. An exception
 411 to this rule is the precision of $\delta^{18}\text{O}$ reconstructions, which decreases with increasing sampling resolution
 412 (see **Fig. 9C-D**). Precision standard deviations of all Δ_{47} -based approaches eventually converge with the
 413 initially much higher precision of $\delta^{18}\text{O}$ reconstructions when sampling resolution increases. However, the
 414 sampling resolution required for Δ_{47} -based reconstructions to rival or outcompete the $\delta^{18}\text{O}$ reconstructions
 415 differs, with **optimization** requiring lower sampling resolutions than the other methods (e.g. 20-40
 416 samples/year compared to 40-80 samples/year for **smoothing** and **binning**; **Fig. 9A-D**). Accuracy also
 417 improves with sampling resolution (**Fig. 9E-H**). When grouping all cases together, it becomes clear that
 418 $\delta^{18}\text{O}$ reconstructions can only approach the accuracy of Δ_{47} -based approaches for reconstructions of MAT.
 419 Seasonality in both SST and $\delta^{18}\text{O}_w$ is most accurately reconstructed using **binning**, and the **smoothing**
 420 approach once again performs worst.

421



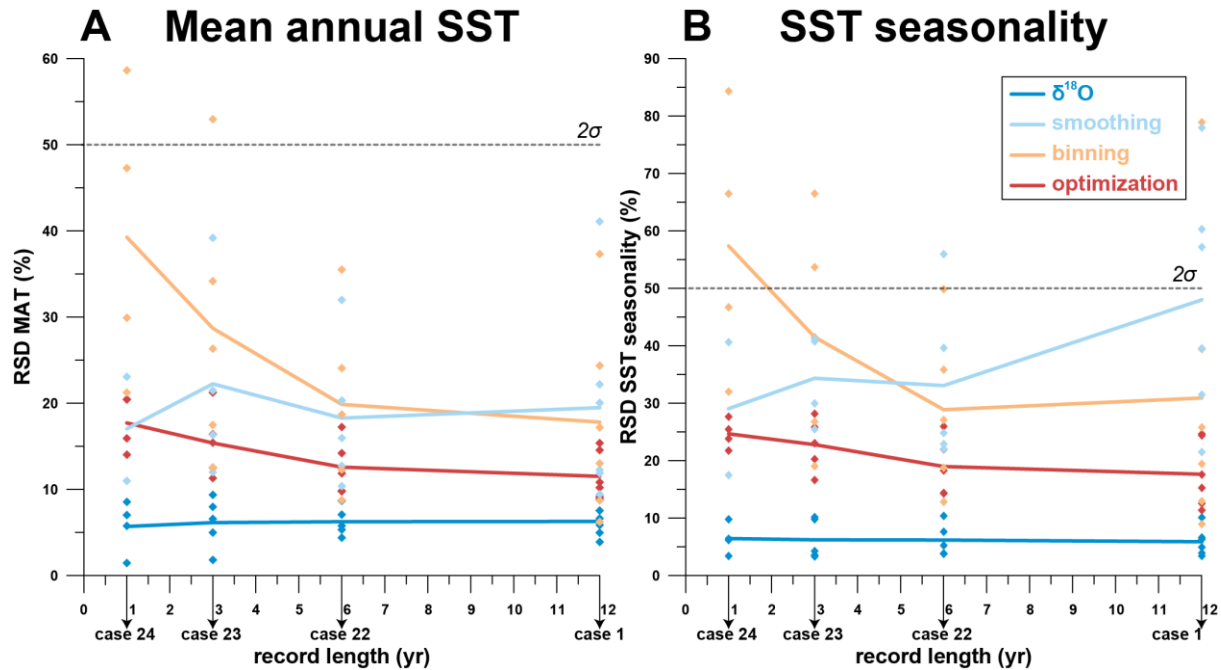
422 **Figure 10:** Effect of SST seasonality range (difference between warmest and coldest month) in the record
 423 on the relative precision of SST seasonality reconstructions (“RSD”, defined as one standard deviation
 424 divided by the mean value). **A** shows precision results if random variability (“weather patterns”) in both SST
 425 and $\delta^{18}\text{O}_w$ as well as measurement uncertainty is added to the records (see 2.3.3 and S1). **B** shows
 426 precision of records with random variability in SST and measurement uncertainty only. **C** shows precision
 427 if only measurement uncertainty is considered. Color coding follows the scheme in **Fig. 1** and **Fig. 4**.
 428 Shaded dots represent results at various sampling resolutions, while bold lines are averages for all
 429 reconstruction approaches. Black circles highlight the places where curves cross the threshold of two
 430 standard deviations, which indicates the minimum SST seasonality that can be resolved within 2 standard
 431 deviations (~95% confidence level) using the reconstruction approach.

432

433 3.4 Resolving SST seasonality

434 Comparison of cases 19, 20 and 21 (SST seasonality of 9.7°C, 5.7°C and 2.1°C respectively) with control
435 case 1 (SST seasonality of 19.3°C) shows how changes in the seasonal SST range affect the precision of
436 measurements (**Fig. 10**; see also **Table 1** and **Supplementary Data S1**). The data reconfirms that $\delta^{18}\text{O}$
437 reconstructions are most precise; a deceptive statistic given the risk of highly inaccurate results this
438 approach yields (see **Fig. 8**). Taking into consideration only analytical uncertainty, all approaches except
439 for **smoothing** can confidently resolve at least the highest SST seasonality within a significance level of
440 two standard deviations (~95%) using a moderate sampling resolution (mean of all resolutions shown in
441 **Fig. 10**). Increasing sampling resolution improves the precision of Δ_{47} -based reconstructions (see **Fig. 9D**),
442 so high sampling resolutions (0.1 or 0.2 mm) allow smaller seasonal differences to be resolved. When
443 random sub-annual variability is added to the SST and $\delta^{18}\text{O}_w$ records (see **2.3.3**), the minimum seasonal
444 SST extent that can be resolved decreases for all approaches (**Fig. 10B** and **10C**). Nevertheless, $\delta^{18}\text{O}$ and
445 **optimization** reconstructions remain able to resolve a relatively small SST seasonality of 2-4°C.

446



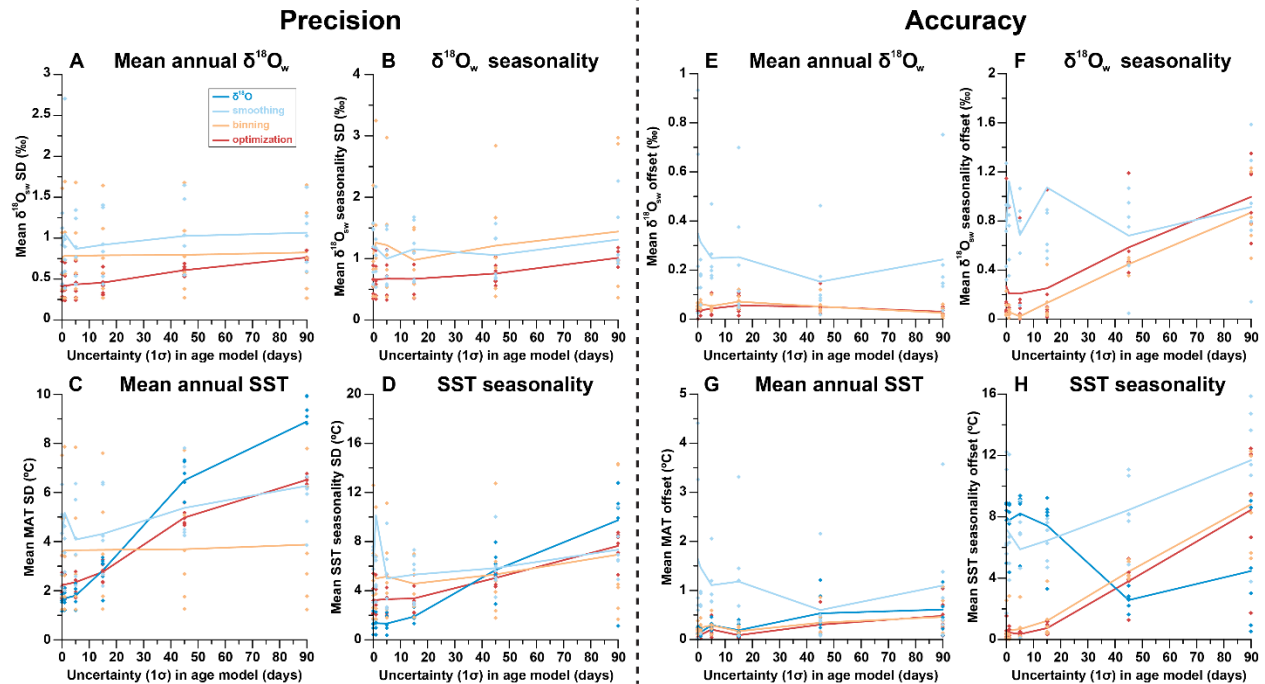
447

448 **Figure 11:** Effect of record length (in years) on the relative precision (one standard deviation as fraction of
 449 the mean value) of results of reconstructions of mean annual SST (A) and SST seasonality (B). Colored
 450 dots represent results for the six different sampling resolutions. Solid lines connect averages for cases 1,
 451 22, 23 and 24 for each reconstruction approach.

452

453 3.5 Effect of record length

454 The effect of variation in the length of the record was investigated by comparing cases 22, 23 and 24 (record
 455 lengths of 6 years, 3 years and 1 year, respectively) with the control case (record length of 12 years; see
 456 **Fig. 11** and **Table 1**). Precision of MAT and SST seasonality reconstructions slightly increase in larger
 457 datasets (longer records) for **optimization** and **binning**, but not for **smoothing** and **δ¹⁸O** reconstructions.
 458 Differences between reconstruction approaches remain relatively constant regardless of the length of the
 459 record, with precision hierarchy generally remaining intact (**δ¹⁸O** > **optimization** > **binning** > **smoothing**).
 460 However, in very short records (1-2 years) **smoothing** generally gains an advantage over other Δ₄₇-based
 461 methods due to its lack of sensitivity to changes in the record length, and **binning** reconstructions are not
 462 precise enough to resolve SST seasonality within two standard deviations (~95% confidence level).
 463 Variation in precision is largely driven by very low precision of reconstructions in records with low sampling
 464 resolutions (sampling intervals of 1.55 mm or 3.25 mm; see also **Fig. 9A-D**). As a result, most of the
 465 reduction in precision in shorter records can be mitigated by denser sampling.



466

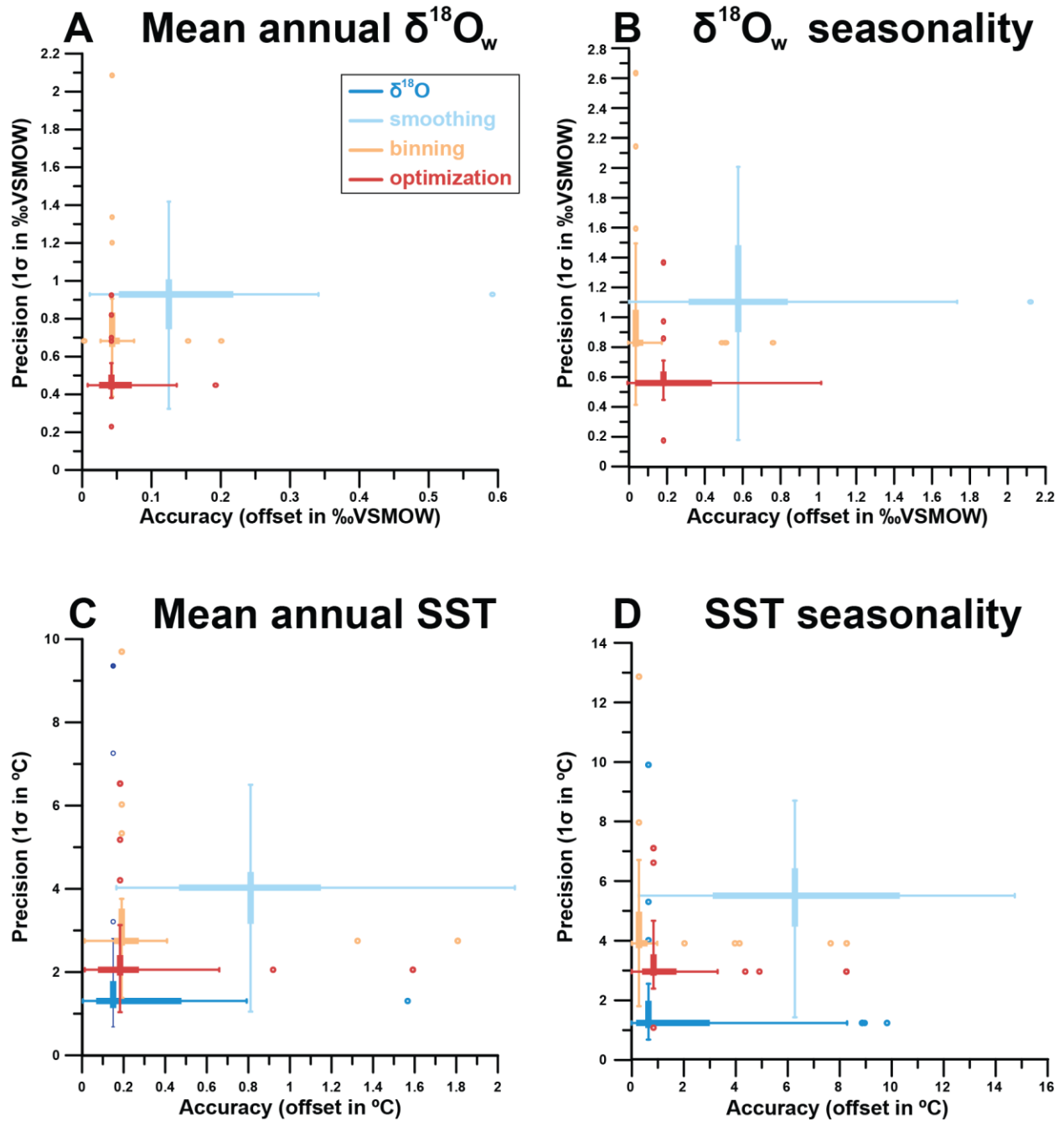
467 **Figure 12:** Effect of uncertainty in age model on the precision (standard deviation on estimate) of results
 468 of reconstructions of mean annual $\delta^{18}\text{O}_w$ (A) and seasonal range in $\delta^{18}\text{O}_w$ (B), mean annual SST (C) and
 469 seasonal range in SST (D). Effect of uncertainty in age model on the accuracy (offset from true value) of
 470 results of reconstructions of mean annual $\delta^{18}\text{O}_w$ (E) and seasonal range in $\delta^{18}\text{O}_w$ (F), mean annual SST
 471 (G) and seasonal range in SST (H). Color coding follows the scheme in Fig. 1 and Fig. 4.

472

473 3.6 Effect of age model uncertainty

474 Uncertainty in the age model has a significant effect on both the precision and the accuracy (Fig. 12) of
 475 reconstructions using all approaches. The $\delta^{18}\text{O}$ reconstructions are most strongly affected by uncertainties
 476 in the age model and suffer from a large decrease in precision with increasing age model uncertainty (Fig.
 477 12C-D). The high precision of the $\delta^{18}\text{O}$ approach in comparison with the Δ_{47} approaches quickly disappears
 478 when age model uncertainty increases beyond 20-30 days. Accuracy of $\delta^{18}\text{O}_c$ -based SST seasonality
 479 reconstructions initially improves with age model uncertainty (Fig. 12H). However, this observation is likely
 480 caused by the fact that age model uncertainty was compared based on conditions in case 9, which features
 481 a phase offset between SST and $\delta^{18}\text{O}_w$ seasonality causing the $\delta^{18}\text{O}$ method to be highly inaccurate even
 482 without age model uncertainty. The precision of **smoothing** and **optimization** approaches also decreases
 483 with increasing age model uncertainty (Fig 12A-D), and the **optimization** approach loses its precision
 484 advantage over the **binning** and **smoothing** approaches when age model uncertainty increases beyond

485 30 days. The monthly **binning** approach is most resilient against increasing age model uncertainty.
486 Seasonality reconstructions through both the **binning** and **optimization** approach quickly lose accuracy
487 when age model uncertainty increases but the accuracy of the **smoothing** approach remains the worst of
488 all Δ_{47} -based approaches in regardless of age model uncertainty except in the case of $\delta^{18}\text{O}_w$ seasonality at
489 exceptionally high (>60 days) age uncertainty (**Fig. 12E-H**).



490

491 **Figure 13:** Overview of averages and ranges of accuracy (absolute offset from real value) and precision
 492 (one standard deviation from the mean) on mean annual $\delta^{18}\text{O}_w$ (A) and seasonal range in $\delta^{18}\text{O}_w$ (B), mean
 493 annual SST (C) and seasonal range in SST (D) within all cases using the four different reconstruction
 494 approaches. Color coding follows the scheme in Fig. 1 and Fig. 4. Box-whisker plots for precision and
 495 accuracy cross at their median values and outliers (colored symbols) are identified based on 2x the
 496 interquartile difference (thick lines).

497

498 4. Discussion

499 4.1 Performance of reconstruction approaches

500 4.1.1 $\delta^{18}\text{O}_c$ vs Δ_{47} -based reconstructions

501 **Figure 13** summarizes the general reliability of the four approaches. $\delta^{18}\text{O}$ reconstructions are generally
502 less accurate than Δ_{47} -based reconstructions (especially **binning** and **optimization**; see also
503 **Supplementary Data S9**). This is a consequence of the assumption that $\delta^{18}\text{O}_w$ remains constant year-
504 round, and that one knows its true value. Both these assumptions are problematic in the absence of
505 independent evidence of the value of $\delta^{18}\text{O}_w$, especially in deep time settings (see e.g. Veizer and Prokoph,
506 2015; Henkes et al., 2018). The risk of this assumption is made clear when comparing cases in which $\delta^{18}\text{O}_w$
507 is indeed constant year-round at the assumed value (0‰; e.g. cases 1-6 and 19-24) with cases in which
508 shifts in $\delta^{18}\text{O}_w$ occur, especially when these shifts are out of phase with respect to the SST seasonality (e.g.
509 cases 9-11, 18 and 25-33; **Fig. 8C-D**). Cases mimicking or based on natural SST and SSS variability (cases
510 14-18 and 30-33) as well as the modern oyster data (**Fig. 6**) yield stronger inaccuracies in MAT and
511 seasonality reconstructions, showing that even in many modern natural circumstances the assumption of
512 constant $\delta^{18}\text{O}_w$ is problematic.

513 It is important to consider that the value of mean annual $\delta^{18}\text{O}_w$ remained very close to the assumed value
514 of 0‰ (within 0.15‰) in all cases except for natural data cases 30 (-1.55‰), 32 (1.01‰; see
515 **Supplementary Data S5**) and the real oyster data (-1.42‰; **Fig. 5**). The SST values of these cases
516 reconstructed using $\delta^{18}\text{O}_c$ data show large offsets from their actual values (+6.7°C, -4.7°C and +10.3°C for
517 case 30, case 32 and the real oyster data respectively; see **Fig. 6 and 8** and **Supplementary Data S5**).
518 These offsets are equivalent to the temperature offset one might expect from inaccurately estimating $\delta^{18}\text{O}_w$
519 (~ -4.6 °C/‰; Kim and O'Neil, 1997) and are only rivaled by the offset in MAT reconstructions of case 18
520 (+5.0°C), which has growth hiatuses obscuring the coldest half of the seasonal cycle. The fact that such
521 differences in $\delta^{18}\text{O}_w$ exist even in modern environments should not come as a surprise, given the available
522 data on worldwide variability of $\delta^{18}\text{O}_w$ (at least -3‰ to +2‰; e.g. LeGrande and Schmidt, 2006) and SSS
523 (30 to 40; ESA, 2020) in modern ocean basins. However, it should warrant caution in using $\delta^{18}\text{O}_c$ data for
524 SST reconstructions even in modern settings. Implications for deep time reconstructions are even greater,

525 given the uncertainty on and variability in global average (let alone local) $\delta^{18}\text{O}_w$ values (Jaffrés et al., 2007;
526 Veizer and Prokoph, 2015). The complications of using $\delta^{18}\text{O}_c$ as a proxy for marine temperatures in deep
527 time are discussed in detail in O'Brien et al. (2017), and Tagliavento et al. (2019). Complications arising
528 from variability in $\delta^{18}\text{O}_w$ are more serious in climate records from euryhaline carbonate producers (e.g.
529 oysters) than from stenohaline organisms (e.g. corals), as they are mainly driven by salinity fluctuations.
530 For example, seasonal salinity variability in the North Sea in offshore sites away from freshwater sources
531 can be as low as 0.25 (Harwood et al., 2008), compared to 3-4 in the coastal Texel site simulated in case
532 30. Given this variability, studies using the $\delta^{18}\text{O}_c$ proxy for SST reconstructions are recommended to either
533 reconstruct $\delta^{18}\text{O}_w$ through additional measurements (e.g. including clumped isotope analysis) or constrain
534 $\delta^{18}\text{O}_w$ variability through isotope-enabled modelling (e.g. Williams et al., 2009)

535 The analytical uncertainty of individual $\delta^{18}\text{O}_c$ aliquots (typically 1 S.D. of 0.05‰; e.g. de Winter et al., 2018)
536 represents only ~1.1% of the variability in $\delta^{18}\text{O}_c$ over the seasonal cycle (~4.3‰ for the default 20°C
537 seasonality in case 1, following Kim and O'Neil, 1997). This is much smaller than the analytical uncertainty
538 of Δ_{47} (typically 1 S.D. of 0.02-0.04‰; e.g. Fernandez et al., 2017; de Winter et al., 2020b), which equates
539 to 25-50% of the seasonal variability in Δ_{47} (~0.08‰ for 20°C seasonality, following Bernasconi et al., 2018;
540 see **Supplementary Data S7**). This roughly 20-fold difference in relative precision causes $\delta^{18}\text{O}_c$ based SST
541 reconstructions to be much more precise (see **Figs 7, 9-12**) than those based on Δ_{47} , and forces the
542 necessity for grouping Δ_{47} data in reconstructions. However, as discussed above, the high precision of $\delta^{18}\text{O}$
543 reconstructions is a misleading statistic if they are highly inaccurate.

544 Our results show that paleoseasonality reconstructions based on $\delta^{18}\text{O}_c$ can only be relied upon if there is
545 strong independent evidence of the value of $\delta^{18}\text{O}_w$ and if significant sub-annual variability in $\delta^{18}\text{O}_w$ (>0.3‰,
546 equivalent to a 2-3°C SST variability; see **Fig. 9-10**; Kim and O'Neil, 1997) can be excluded with confidence.
547 Examples of such cases include fully marine environments unaffected by influxes of (isotopically light)
548 freshwater or evaporation (increasing $\delta^{18}\text{O}_w$; Rohling, 2013). Carbonate records from environments with
549 more stable $\delta^{18}\text{O}_w$ conditions include, for example, the *A. islandica* bivalves from considerable depth (30-
550 50m) in the open marine Northern Atlantic (e.g. Schöne et al., 2005, on which case 33 is based). However,
551 even here variability in $\delta^{18}\text{O}_{sw}$ due to, for example, shifting influence of different bottom water masses

552 cannot be fully excluded. Previous reconstruction studies show that $\delta^{18}\text{O}_w$ in smaller basins are heavily
553 influenced by the processes affecting $\delta^{18}\text{O}_w$ on smaller scales, such as local evaporation and freshwater
554 influx from nearby rivers (e.g. Surge et al., 2001; Petersen et al., 2016). Consequently, accurate quantitative
555 reconstructions of seasonal range in shallow marine environments with extreme seasonality may not be
556 feasible using the $\delta^{18}\text{O}$ approach, because these environments are invariably characterized by significant
557 fluctuations in $\delta^{18}\text{O}_w$ and growth rate.

558 While variability in $\delta^{18}\text{O}_w$ compromises accurate $\delta^{18}\text{O}$ -based seasonality reconstructions, the compilation
559 in **Fig. 3** shows that its influence on the $\delta^{18}\text{O}$ records is too small to affect the shape of the record to such
560 a degree that seasonality is fully obscured. While natural situations with $\delta^{18}\text{O}_w$ fluctuations large enough to
561 totally counterbalance the effect of temperature seasonality on $\delta^{18}\text{O}$ records are imaginable, these cases
562 are likely rare. This means that chronologies based on $\delta^{18}\text{O}$ seasonality, which are a useful tool to anchor
563 seasonal variability in absence of independent growth markers (e.g. Judd et al., 2018; de Winter, 2021b),
564 are reliable in most natural cases.

565 *4.1.2 Seasonality reconstructions using moving averages (smoothing)*

566 Of the three methods for combining Δ_{47} data, the **smoothing** approach clearly performs worst in all four
567 reconstructed parameters (MAT, SST seasonality, mean annual $\delta^{18}\text{O}_w$ and $\delta^{18}\text{O}_w$ seasonality), both in
568 terms of accuracy and precision (**Fig. 13**). While applying a moving average may be a good strategy for
569 lowering the uncertainty of Δ_{47} -based temperature reconstructions in a long time series (e.g. Rodríguez-
570 Sanz et al., 2017), the method underperforms in cases where baseline and amplitude of a periodic
571 component (e.g. MAT and SST seasonality) are extracted from a record. This is likely due to the smoothing
572 effect of the moving average, which reduces the seasonal cycle and causes highly inaccurate seasonality
573 reconstructions (offsets mounting to $>6^\circ\text{C}$; **Fig. 13**). This bias is especially detrimental in cases where the
574 seasonal cycle is obscured by seasonal growth halts (e.g. case 18), multi-annual trends in growth (e.g.
575 case 4, 14 and 17) and multi-annual trends in SST (e.g. case 15 and 17; see **Fig. 7 and 8**). The poor
576 performance of the **smoothing** approach can be slightly mitigated by increasing sampling resolution (**Fig**
577 **9**), but even at high sampling resolutions (every 0.1 or 0.2 mm) the method still fails to reliably resolve
578 seasonal SST ranges below 5°C even in idealized cases (case 19-21; **Fig. 10**). Increasing the number of

579 samples by analyzing longer records does not improve the result, because smoothing of the seasonal cycle
580 by a moving average window introduces the same dampening bias if the temporal sampling resolution
581 (number of samples per year) remains equal (**Fig. 11**).

582 More critically, employing the **smoothing** method may give the illusion that seasonality is more reduced,
583 and severely bias reconstructions. This bias highlights the importance of using the official meteorological
584 definition of seasonality as the difference between the averages of warmest and coldest month in
585 paleoseasonality work (O'Donnell and Ignizio, 2012). This definition is much more robust than the “annual
586 range” often cited based on maxima and minima in $\delta^{18}\text{O}_c$ records. This “annual range” strongly depends on
587 sampling resolution, which is typically <12 samples/yr (Goodwin et al., 2003), equivalent to the third lowest
588 sampling interval (0.75 mm) simulated in this study. Therefore, we strongly recommend future studies to
589 adhere to the monthly definition of seasonality to foster comparison between studies. While inter-annual
590 variability is lost by combining data from multiple years into monthly averages, this approach increases
591 precision, accuracy and comparability of paleoseasonality results. Inter-annual variability can still be
592 discussed from plots of raw data plotted in time or sampling domain.

593 *4.1.3 Monthly **binning**, sample size **optimization** and age model uncertainty*

594 Overall, the most reliable paleoseasonality reconstructions can be obtained from either **binning** or
595 **optimization** (**Fig. 13**). In general, **optimization** is slightly more precise, while **binning** yields more
596 accurate estimates of seasonal range in SST and $\delta^{18}\text{O}_w$ (**Fig. 13B and D**). The more flexible combination
597 of aliquots in the **optimization** routine yields improved precision (especially on mean annual averages) in
598 cases where parts of the record are undersampled or affected by hiatuses and simultaneous fluctuations
599 in both SST and $\delta^{18}\text{O}_w$ (e.g. case 3-6, 14-18, 30-33). The downside of this flexibility is that in the case of
600 larger sample sizes, the seasonal variability may be dampened, like in the **smoothing** approach (see **4.1.2**).
601 This apparent dampening effect may be reduced by allowing the sample size of summer and winter samples
602 to vary independently in the **optimization** routine, at the cost of higher computational intensity due to the
603 larger number of sample size combinations (see 2.1 and 4.2.2). The rigid grouping of data in monthly bins
604 in **binning** prevents this dampening and therefore yields slightly more accurate estimates of seasonal
605 ranges in SST and $\delta^{18}\text{O}_w$. A caveat of **binning** is that it requires a very reliable age model of the record, at

606 least on a monthly scale. If the age model has a large uncertainty, there is a risk that samples are grouped
607 in the wrong month, which compromises the accuracy of **binning** reconstructions, especially for
608 reconstructions of seasonal range (**Fig 12H**). This problem is exacerbated by potential phase shifts between
609 seasonality in paleoclimate variables (SST and $\delta^{18}\text{O}_w$) and calendar dates, which may occur in the presence
610 of a reliable age model.

611 Previous authors attempted to circumvent the dating problem by analyzing high-resolution $\delta^{18}\text{O}_c$ transects
612 and subsequently sampling the seasonal extremes for clumped isotope analyses (Keating-Bitonti et al.,
613 2011; Briard et al., 2020). While this approach does not require sub-annual age models, it has several
614 disadvantages compared with the **binning** and **optimization** approaches: Firstly, it requires separate
615 sampling for $\delta^{18}\text{O}_c$ and Δ_{47} , which may not be possible in high-resolution carbonate archives due to sample
616 size limitations. Analyzing small aliquots for combined $\delta^{18}\text{O}_c$ and Δ_{47} analyses consumes less material.
617 Secondly, individual summer and winter temperature reconstructions require large (> 1.5 mg; e.g.
618 Fernandez et al., 2017) Δ_{47} samples from seasonal extremes, which causes more time-averaging than the
619 approaches combining small aliquots. Finally, the position of seasonal extremes estimated from the $\delta^{18}\text{O}_c$
620 record may not reflect the true seasonal extent if seasonal SST and $\delta^{18}\text{O}_w$ cycles are not in phase (as in
621 case 9), causing the seasonal Δ_{47} -based SST reconstructions to underestimate the temperature
622 seasonality. In such cases, $\delta^{18}\text{O}_c$ and Δ_{47} analyses on small aliquots allow the seasonality in SST and $\delta^{18}\text{O}_w$
623 to be disentangled, yielding more accurate seasonality reconstructions.

624 Techniques for establishing independent age models for climate archives range from counting of growth
625 layers or increments (Schöne et al., 2008; Huyghe et al., 2019), modelling and extracting of rhythmic
626 variability in climate proxies through statistical approaches (e.g. De Ridder et al., 2007; Goodwin et al.,
627 2009; Judd et al., 2018; de Winter, 2021b) and interpolation of uncertainty on absolute dates (e.g. Scholz
628 and Hoffman, 2011; Meyers, 2019; Sinnesael et al., 2019). While propagating uncertainty in the data on
629 which age models are based onto the age model is relatively straightforward, errors on underlying *a priori*
630 assumptions such as linear growth rate between dated intervals, (quasi-)sinusoidal forcing of climate cycles
631 and the uncertainty on human-generated data such as layer counting are very difficult to quantify (e.g.
632 Comboul et al., 2014) and may not be normally distributed. Results of cases 25-29 show that uncertainties

633 in the age domain can significantly compromise reconstructions (**Fig. 12**). Within the scope of this study,
634 only the effect of symmetrical, normally distributed uncertainties on an artificial case with phase decoupled
635 SST and $\delta^{18}\text{O}_w$ seasonality (case 9) was tested. The effects of other types of uncertainties on the
636 reconstructions remain unknown, highlighting an unknown uncertainty in paleoseasonality and other high-
637 resolution paleoclimate studies that may introduce bias or lead to over-optimistic uncertainties on
638 reconstructions. Future research could quantify this unknown uncertainty by propagating estimates of
639 various types of uncertainty on depth values of samples and on the conversion from sampling to time
640 domain in age models.

641 **4.2 Conditions influencing success of reconstructions**

642 The reliability (accuracy and precision) of SST and $\delta^{18}\text{O}_w$ reconstructions depend on case-specific
643 conditions. The range of case studies tested in this study allowed us to evaluate the effect of variability in
644 SST, growth rate, $\delta^{18}\text{O}_w$, sampling resolution and record length relative to the control case (case 1; see
645 **Supplementary Data S1**). A summary of the effects of these changes is given in **Table 2**.

646

Variable	cases	Metric	Effect on reconstructions			
			$\delta^{18}\text{O}$	smoothing	binning	optimization
SST	12	Precision	0	+++	+	0
	15					
	17					
	19-21 30-33	Accuracy	+	+	0	+
Growth rate	2-6	Precision	+	++	++	+
	14-18					
	30-33	Accuracy	+	++	0	+
$\delta^{18}\text{O}_w$	7-11	Precision	+	++	0	0
	13-18					
	30-33	Accuracy	+++	+++	+	++
Sampling resolution	1-33	Precision	0	+++	++	++
		Accuracy	+	+	+++	+
Record length	22-24	Precision	0	0	+++	++
		Accuracy	+	0	++	++
Age model uncertainty?	25-29	Precision	+++	++	0	++
		Accuracy	+	+	++	++

647 **Table 2:** Qualitative summary of the effects of changes in variables relative from the ideal case on
648 reconstructions using the four approaches. The “cases” column lists cases in which the changes in the
649 respective variable relative to the control case (case 1) were represented (see **Table 1** and **S1**). “0” =
650 negligible effect, “+” = weak increase in uncertainty, “++” = moderate increase in uncertainty, “+++” = strong
651 increase in uncertainty. Precision and accuracy of all tests is given in **S9**.

652

653 4.2.1 SST variability

654 Variability in water temperature most directly affects the proxies under study. By default (case 1), SST
655 varies sinusoidally around a MAT of 20°C with an amplitude of 10°C (see **2.3.3**, **Fig. 2** and **Supplementary**
656 **Data S1**). In cases in which multi-annual variability in SST is simulated (e.g. case 15 and 17), the accuracy
657 of SST reconstructions using $\delta^{18}\text{O}$ and **optimization** are reduced, while the **binning** approach is less
658 strongly affected. Examples of such multi-annual cyclicity are El-Niño Southern Oscillation (ENSO;
659 Philander, 1983) or North Atlantic Oscillation (NOA; Hurrell, 1995). The effect is especially large in case 17,
660 which simulates a tropical environment with reduced SST seasonality and a strong multi-annual cyclicity.
661 This type of environment is analogous to the environment of tropical shallow water corals, which are often
662 used as archives for ENSO variability (e.g. Charles et al., 1997; Fairbanks et al., 1997) and is similar to
663 tropical cases from the Australian Great Barrier Reef (case 31) and Red Sea (case 32; see **Fig. 3**). We
664 therefore recommend using the **binning** approach on carbonate records where multi-annual cyclicity is

665 prevalent and if a reliable age model can be established for these records (as in e.g. Sato, 1999; Scourse
666 et al., 2006; Miyaji et al., 2010).

667 *4.2.2 Growth rate variability and hiatuses*

668 **Figures 7 and 8** show that variations in the growth rate of records, including the occurrence of hiatuses,
669 have a strong effect on reconstructions, especially using the **smoothing** approach. In general, hiatuses
670 and slower growth reduce precision of monthly SST and $\delta^{18}\text{O}_w$ reconstructions by reducing mean temporal
671 sampling resolution (samples/yr; see **Fig. 9**), and because parts of the record are undersampled. The effect
672 on accuracy depends strongly on the timing of changes in growth rate or the occurrence of hiatuses. Cases
673 2-6 simulate specific growth rate effects and can be used to test these differences. The **smoothing** method
674 is especially sensitive to changes in growth rate that take place in specific seasons, such as hiatuses in
675 winter (case 2) or summer (case 3) and growth peaks in summer (case 5) or spring (case 6). The other
676 reconstruction approaches are less affected by this bias, because they generally do not mix samples from
677 different seasons. The $\delta^{18}\text{O}$ method is especially well suited to deal with changes in growth rate because
678 it does not require combining different aliquots for accurate SST reconstructions. The **binning** and
679 **optimization** approaches are slightly less reliable in cases where growth rate decreases linearly or
680 seasonally along the entire record (cases 4-6; **Fig. 2**). Because these two methods consider all samples in
681 the records at once, they are more sensitive to changes in temporal sampling resolution along the record.
682 It is worth noting that **optimization** is especially sensitive to sharp changes in growth rate in summer (e.g.
683 cases 11, 14, 16 and 17) because those conditions force the **optimization** routine to use larger sample
684 sizes or include samples outside the warmest month for summer temperature estimates. A potential solution
685 to this problem could be to allow sample sizes of summer and winter groups to vary independently in the
686 **optimization** routine (see 2.1). This would allow sample size in the undersampled season (in this case:
687 summer) to become larger than that at the other end of the $\delta^{18}\text{O}_c$ spectrum, reducing uncertainty on the
688 more densely sampled season and therefore improving the entire seasonality reconstruction.

689 A worst-case scenario is represented by case 18, where the cold half of the year is not recorded. Such
690 cases result in strong biases in reconstructions of mean annual and seasonal ranges in SST and $\delta^{18}\text{O}_w$,
691 regardless of which method is used. In such extreme cases the record simply contains insufficient

692 information to reconstruct variability in growth rate, SST and $\delta^{18}\text{O}_w$, and it seems that no statistical method
693 would enable this missing information to be recovered. The solution for these reconstructions would be to
694 establish reliable age models, independent of $\delta^{18}\text{O}$ or Δ_{47} data, which show that a large part of the seasonal
695 cycle is missing. All methods used in this study rely on a conversion of SST and $\delta^{18}\text{O}_w$ reconstructions to
696 the time domain to define monthly time bins. This conversion breaks down in fossil examples when the
697 seasonal cycle cannot be extracted from the archive, which happens when half of the seasonal cycle or
698 more is obscured by growth hiatuses, as exemplified in case 18.

699 While hiatuses encompassing half of the seasonal cycle are uncommon, changes in growth rate are
700 common in accretionary carbonate archives because conditions for (biotic or abiotic) carbonate
701 mineralization often vary over time. This variability is either driven by biological constraints, such as
702 senescence (e.g. Schöne, 2008; Hendriks et al., 2012), the reproductive cycle (Gaspar et al., 1999) or
703 stress (Surge et al., 2001; Compton et al., 2007) or by variations in the environment that promote or inhibit
704 carbonate production, such as seasonal variations in temperature (Crossland, 1984; Bahr et al., 2017) or
705 precipitation (Dayem et al., 2010; Van Rangelbergh et al., 2014). In general, such conditions occur more
706 frequently in mid- to high-latitude environments than in low-latitudes, and in more coastal environments
707 rather than in open marine settings, because these environments contain stronger variations in the factors
708 that influence growth rates (e.g. temperature, precipitation or freshwater influx; e.g. Surge et al., 2001;
709 Ullmann et al., 2010). This difference was simulated in the cases representing natural variability (case 14-
710 18 and 30-33). Accuracy in the coastal high-latitude settings (cases 16, 18 and 29) are indeed more strongly
711 affected by changes in growth rate. Because in such highly variable environments growth rate variability
712 often co-occurs with variability in $\delta^{18}\text{O}_w$, using $\delta^{18}\text{O}_c$ -based reconstructions is not advised, unless $\delta^{18}\text{O}_w$
713 variability can be constrained or neglected (which is rare in these environments).

714 Additional complications include the lack of constraint on growth rate variability because of uncertainties in
715 the record's age model (see **4.1.3**) and the effect of growth rate variability on the sampling resolution. The
716 effect of growth rate on time-averaging within samples was not specifically tested in this study but
717 introduces uncertainty in practice when archives with variable growth rate are sampled at a constant
718 sampling resolution in the depth domain. In this case, parts of the archive with a lower growth rate yield

719 more time-averaged samples, potentially dampening one extreme of the seasonal cycle (e.g. Goodwin et
720 al., 2003). In highly dynamic environments it is challenging to isolate all variables that introduce bias, and
721 irregular variability in growth rate and $\delta^{18}\text{O}_w$ will invariably introduce uncertainty in SST reconstructions,
722 even when applying the best Δ_{47} -based approaches (e.g. **binning** and **optimization**). In such examples,
723 the results of natural variability cases (14-18 and 30-33) and of the real oyster data (**Fig. 6**) serve as
724 benchmarks for the degree of uncertainty that may remain unexplained in these records.

725 *4.2.3 Variability in $\delta^{18}\text{O}_w$*

726 As discussed in **4.1.1**, these variations in $\delta^{18}\text{O}_w$ have a large effect on the accuracy of $\delta^{18}\text{O}_c$ -based
727 reconstructions, and their occurrence constitutes the main advantage of applying the Δ_{47} thermometer
728 (Eiler, 2011). However, results of cases 7-11 in **Fig. 8** and **Table 2** show that $\delta^{18}\text{O}_w$ variations can also bias
729 Δ_{47} -based reconstructions, especially those of seasonal ranges and those using the **smoothing** approach.
730 **Smoothing** reconstructions are biased by these $\delta^{18}\text{O}_w$ shifts in much the same way as they are affected
731 by shifts in growth rate (see **4.2.2**). The **optimization** approach is sensitive to seasonal changes in $\delta^{18}\text{O}_w$
732 in antiphase with SST seasonality and by increases in $\delta^{18}\text{O}_w$ in summer (e.g. due to excess evaporation;
733 e.g. case 11), especially when used for reconstructions of $\delta^{18}\text{O}_w$ seasonality. This effect arises because
734 the **optimization** approach orders data based on $\delta^{18}\text{O}_c$ and Δ_{47} seasonality to isolate the $\delta^{18}\text{O}_w$ -SST
735 relationship. Both antiphase $\delta^{18}\text{O}_w$ seasonality and summer evaporation dampen the seasonal $\delta^{18}\text{O}_c$ cycle
736 and therefore influence the reconstruction of the $\delta^{18}\text{O}_w$ -SST relationship. A good example of this is seen in
737 the real oyster data (**Fig. 6**), where $\delta^{18}\text{O}_w$ and SST vary in phase and $\delta^{18}\text{O}_w$ dampens the SST seasonality.
738 The **binning** approach is more robust against $\delta^{18}\text{O}_w$ variability that dampens the seasonal cycle and is
739 therefore a better choice for absolute SST reconstructions in environments where summer evaporation or
740 other $\delta^{18}\text{O}_w$ variability in phase with SST seasonality is expected to occur, if the age model is reliable
741 enough to allow monthly binning of raw data (see **4.1.3**). Indeed, reconstructions from the lagoonal
742 environment (case 16) and Red Sea case (case 32 which is characterized by strong summer evaporation;
743 e.g. Titschack et al., 2010) show that **binning** is the most reliable choice in these environments.

744 *4.2.4 Variability in sampling resolution and record length*

745 Other factors influencing the effectiveness of reconstructions are the sampling resolution and the length of
746 the record. Many of the cases discussed in this study represent idealized cases with comparatively high
747 sampling resolutions over comparatively long (12 yr) paleoseasonality records, which yield large sample
748 sizes. By comparison, the typical age of mollusks, which are often used as paleoseasonality archives, is 2-
749 5 years (Ivany, 2012). Records with the highest sampling resolutions (0.1 and 0.2 mm) contain up to 1200
750 samples. Generating such records is not impossible, but it is highly unlikely to be applied in paleoclimate
751 studies given the limitation of resources (e.g. instrument time) and the desire to analyze multiple records
752 from different specimens, species, localities or ages to gain a better understanding of the variability in
753 paleoseasonality (e.g. Goodwin et al., 2003; Schöne et al., 2006; Petersen et al., 2016). In some cases
754 large datasets are meticulously collected from single carbonate records (e.g. Schöne et al., 2005;
755 Vansteenberghe et al., 2016; de Winter et al., 2020a; Shao et al., 2020). However, in such studies, the aim
756 is often to investigate variability at a higher (e.g. daily; de Winter et al., 2020a) resolution or longer
757 timescales (e.g. decadal to millennial; Schöne et al., 2005; Vansteenberghe et al., 2016; Shao et al., 2020)
758 in addition to the seasonal cycle, rather than to improve the reliability of reconstructing one type of variability
759 (e.g. seasonality) alone.

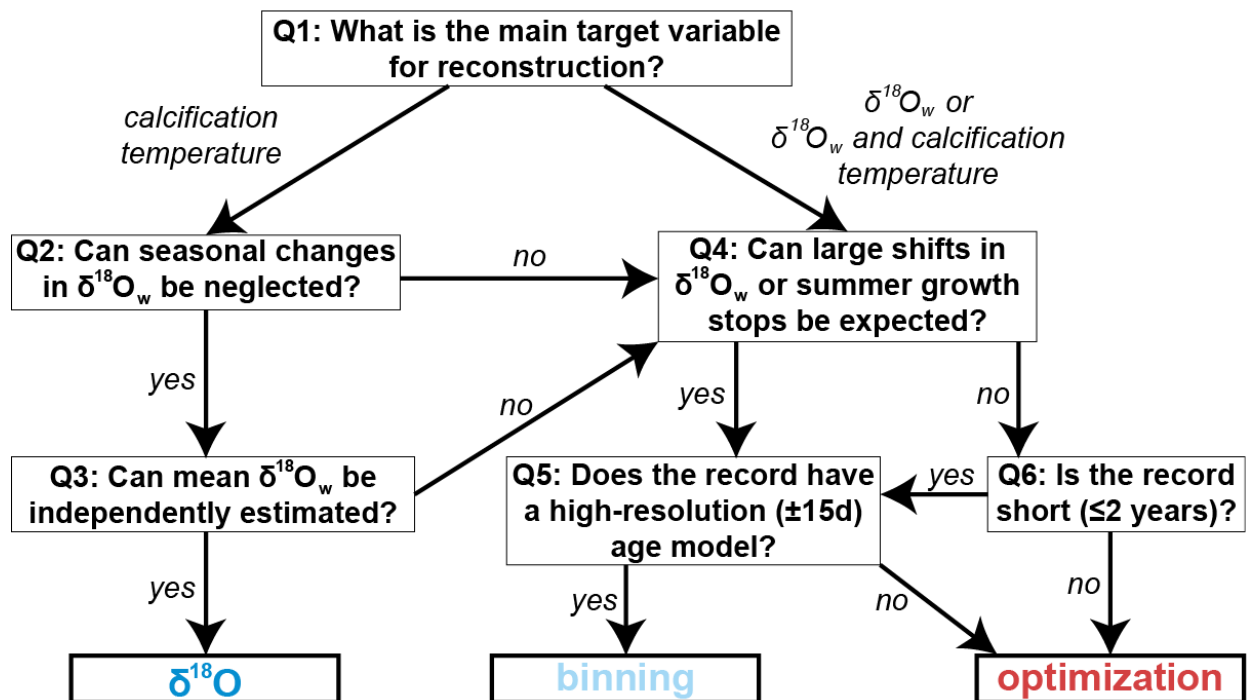
760 **Fig. 9** shows that increasing temporal sampling resolution (samples/yr) improves both the accuracy and
761 precision of all Δ_{47} -based reconstructions. This occurs because Δ_{47} samples have a large analytical
762 uncertainty (see **4.1.2**) and grouping of data therefore improves reconstructions. The decrease in precision
763 of $\delta^{18}\text{O}_c$ -based reconstructions (**Fig. 9C-D**) is explained by the fact that the analytical uncertainty of $\delta^{18}\text{O}_c$
764 measurements is much smaller than the variability introduced by natural sub-annual variability in SST and
765 $\delta^{18}\text{O}_w$ unrelated to the seasonal cycle (see **Supplementary Data S4**). Therefore, higher sampling
766 resolutions allow $\delta^{18}\text{O}_c$ records to better capture this sub-seasonal variability, which introduces more noise
767 to the seasonal cycle (reducing precision) but causes monthly mean SST and $\delta^{18}\text{O}_w$ to be more accurately
768 reconstructed. Towards higher sampling resolutions, the gap in precision between $\delta^{18}\text{O}_c$ - and Δ_{47} -based
769 reconstructions closes, eventually (in an ideal case) diminishing the advantage of high analytical precision
770 in $\delta^{18}\text{O}_c$ measurements (**Fig. 9C-D**).

771 An optimum sample resolution can be defined for each method after which improving sampling resolution
772 does not significantly improve the reliability of the reconstruction (as in de Winter et al., 2017). **Figure 9**
773 shows that this optimum varies depending on which variable (MAT, SST seasonality, mean annual $\delta^{18}\text{O}_w$
774 or $\delta^{18}\text{O}_w$ seasonality) is reconstructed. Therefore, **Fig. 9** will allow future researchers to determine the
775 sampling resolution that is tailored to their purpose. In general, the improvement after a sample size of 20-
776 30 samples per year is negligible for the **binning** and **optimization** methods if the total number of samples
777 (depending on both sampling resolution and record length) is sufficient for monthly temperature
778 reconstructions. Our data show that 200-250 paired $\delta^{18}\text{O}_c$ and Δ_{47} measurements are in general sufficient
779 for a standard deviation of 2-3°C on monthly SST reconstructions using the **binning** or **optimization**
780 approach, preferably when spread over multiple growth years to eliminate the effect of short-term weather
781 events or years with exceptional seasonality (**Fig. 10; Supplementary Data S5**).

782 Record length only has a minimal influence on the **optimization** method but for very short records (≤ 2
783 years) **binning** becomes very imprecise, especially at low sampling resolutions (**Fig. 11**). The reason is
784 that the sample size within monthly time bins becomes too small in these cases, while the more flexible
785 sample size window of the optimization routine circumvents this problem. The choice between these two
786 approaches should therefore be based on a tradeoff between the length of the record (in time) and the
787 number of samples that can be retrieved from it. As a result, shorter-lived, fast-growing climate archives,
788 such as large or fast-growing (e.g. juvenile) mollusk shells, are best sampled using a high temporal
789 resolution (>30 samples/yr) sampling strategy with the **optimization** approach. Longer lived archives with
790 a lower mineralization rate, such as annually laminated speleothems, corals and gerontic mollusks, are
791 best sampled using long time series at monthly resolution using the **binning** approach.

792 A simplified decision tree that could guide sampling strategies for future paleoseasonality studies is shown
793 in **Figure 14**. Note that choices and tradeoffs for these reconstructions may differ depending on the archive
794 and environment in which it formed (see discussion above).

Schematic guide to reconstructing SST and $\delta^{18}\text{O}_w$ from accretionary carbonate archives



795

796 **Figure 15:** Schematic guide to choosing the right approach for reconstructing annual mean or seasonality
 797 in SST and $\delta^{18}\text{O}_w$ from accretionary carbonate archives. Recommendations are based on the results of
 798 testing all four approaches on the entire range of cases. Researchers can follow the six steps (questions
 799 Q1-6) to decide on the right approach for reconstructing the target variable. Guidelines are based on
 800 maximizing both accuracy and precision (see details in **Supplementary Data S9**). Note that the **smoothing**
 801 approach is never the best choice. The choice between the two remaining Δ_{47} -based approaches (**binning**
 802 and **optimization**) relies heavily on the situation and may be driven by a preference for more accurate or
 803 more precise results.

804

805 4.3 Implications for clumped isotope sample size

806 The **optimization** technique for grouping Δ_{47} aliquots for accurate SST and $\delta^{18}\text{O}_w$ reconstructions allows
 807 us to assess the limitations of the clumped isotope thermometer for temperature reconstructions from high-
 808 resolution carbonate archives. The optimal sample size given by the approach is different for different cases
 809 and depends on the temporal sampling resolution and the characteristics of the record (see **S4**). As
 810 expected, in cases more like the ideal case (case 1), optimal sample sizes are low (~14-24), while sample
 811 sizes increase in more complicated cases based on simulated natural environments (case 14-18) or cases
 812 based on actual SST and SSS data (cases 30-33). More confined SST seasonality (cases 19-21) also

813 requires larger samples to reconstruct (up to 100 samples in some cases). This is not surprising, because
814 variability within samples will increase in records in which the seasonality is smaller or more obscured by
815 other environmental variability. The optimal sample size between cases and sampling resolutions is not
816 normally distributed but tails towards high sample sizes with some extreme outliers (Shapiro Wilk test $p <<$
817 0.05; **Supplementary Data S10**). The median sample size of all our simulations is 17 aliquots. This number
818 lies between the minimum number of 14 ~100 μg replicates of standards calculated by Fernandez et al.
819 (2017) and the minimum of 20-40 ~100 μg aliquots required for optimal paleoseasonality reconstruction
820 from fossil bivalves by de Winter et al. (2020b). This is to be expected since many of the cases explored in
821 this study represent ideal cases compared with the natural situation. However, in these virtual cases a
822 measure of random sub-annual variability in SST and $\delta^{18}\text{O}_w$ was added (see **Fig. 4** and **Supplementary**
823 **Data S2**), simulating a more realistic environment and resulting in poorer precision than replicates of a
824 carbonate standard (as in Fernandez et al., 2017). Our simulations show that the optimum number of
825 samples to be combined in seasonality studies depends on both the analytical uncertainty of Δ_{47}
826 measurements (as represented by the estimate in Fernandez et al., 2017) and the variability between
827 aliquots pooled within a sample that is attributed to actual variability within the record (as represented by
828 our simulations and the estimate in de Winter et al., 2020b). The optimal sample size is therefore a good
829 measure for the limitations of temperature variability that can be resolved in a record and can help
830 researchers decide which strategy to apply for combining measurements to obtain the most reliable
831 paleoseasonality estimates, or to decide whether extra sampling is required, even if the chosen approach
832 is not to use the **optimization** routine itself. Note that the optimum sample size is kept equal for summer
833 and winter samples in this study, and that the **optimization** approach can likely achieve better performance
834 by considering unequal sample sizes in opposite seasons (see **4.1.3** and **4.2.2**). While this added flexibility
835 comes at a higher computational cost due to the increased number of possible sample size combinations
836 to be considered, future studies should investigate whether this updated **optimization** approach could yield
837 more reliable seasonality reconstructions.

838 **4.4 Implications for other sample size problems**

839 While the discussion above focuses on optimizing approaches for combining samples for clumped
840 isotope analyses in paleoseasonality reconstructions, the problem of combining samples to reduce
841 uncertainty and isolate variation in datasets is very common (e.g. Zhang et al., 2004; Merz and Thieken,
842 2005; Tsukakoshi, 2011). Therefore, the approaches outlined and tested in this study have applications
843 beyond paleoseasonality reconstructions. Examples of other problems that could benefit from applying
844 similar approaches for reducing the uncertainty of estimates of target variables while minimizing the
845 number of analyses required to meet analytical requirements include: (1) reconstructing
846 paleoenvironmental variability in the terrestrial realm from tooth bioapatite (e.g. Passey and Cerling,
847 2002; Kohn, 2004; Van Dam and Reichart, 2009; de Winter et al., 2016), (2) quantitative time series
848 analysis of orbital cycles in stratigraphic records (e.g. Lourens et al., 2010; de Vleeschouwer et al., 2017;
849 Noorbergen et al., 2018; Westerhold et al., 2020), (3) strontium isotope dating (e.g. McArthur et al., 2012;
850 de Winter et al., 2020c), (4) reconstructing sub-seasonal variability from ultra-high-resolution records (e.g.
851 from fast-growing mollusks and gastropods; e.g. Sano et al., 2012; Warter and Müller, 2017, de Winter et
852 al., 2020d; Yan et al., 2020), and (5) reconstructing sea surface and deep-sea temperatures across short-
853 lived (10–100 kyr) episodes of climate change or climate shifts from deep marine archives characterized
854 by low sedimentation rates (e.g. Lear et al., 2008; Jenkyns, 2010; Stap et al., 2010; Lauretano et al.,
855 2018). A more detailed discussion of the implications for other sample size problems is provided in the
856 **Supplementary Information.**

857

858 5. Conclusions and recommendations

859 The performance of three Δ_{47} -based approaches to reconstruct seasonality from accretionary carbonate
860 archives was evaluated in comparison with conventional $\delta^{18}\text{O}_c$ -based reconstructions in a wide range of
861 case studies. From the results, we conclude that while $\delta^{18}\text{O}_c$ -based reconstructions (**$\delta^{18}\text{O}$**) yield superior
862 precision for SST reconstructions, this method runs a high risk of yielding inaccurate results due to innate
863 assumptions about the value of $\delta^{18}\text{O}_w$, which must be estimated and assumed constant year-round. Unless
864 $\delta^{18}\text{O}_w$ can be independently constrained or variability in $\delta^{18}\text{O}_w$ can be neglected, Δ_{47} -based reconstructions
865 should be the method of choice for absolute mean annual temperature and SST seasonality
866 reconstructions. Various techniques for combining Δ_{47} data were evaluated. Our findings suggest that
867 smoothing Δ_{47} data using a moving average almost always results in a dampening of the seasonal cycle
868 which severely hampers recovery of seasonality. Applying the **smoothing** approach results in inaccuracies
869 in reconstructions of MAT as well, especially in cases where part of the seasonal cycle is obscured by
870 variability in growth rate or multi-annual trends. More reliable seasonality reconstructions are achieved with
871 two approaches for combining Δ_{47} data using time binning (**binning**) or applying a flexible sample size
872 optimization (**optimization**) approach. Of these two approaches, **optimization** achieves better precision
873 and can resolve smaller seasonal temperature differences with confidence. However, **binning** is often more
874 accurate, and outperforms **optimization** as the most reliable approach. This is especially true in cases with
875 growth stops or $\delta^{18}\text{O}_w$ changes in phase with temperature seasonality (e.g. strong seasonal evaporation or
876 freshwater influx) and in longer multi-annual time series with a reliable age model. **Optimization** is the
877 better choice for shorter (<3 years) records, especially if the sampling resolution can be increased, such as
878 in short, fast growing climate archives.

879 Despite the focus on the problem of resolving seasonality in carbonate archives, the findings in this study
880 have applications for other problems in earth science where sample size and sampling resolution put limits
881 on the ability to resolve specific trends, events, and cycles from time series. While the above-mentioned
882 recommendations of the **optimization** and **binning** methods are likely valid for most studies aiming to
883 quantify the mean and amplitude of a specific cycle or event (equivalent to MAT and SST seasonality),

884 (dynamic) moving averages (**smoothing**) are expected to yield the best results in studies quantifying
885 aperiodic trends from longer data series.

886

887 **Code availability**

888 All scripts used to make the calculations described in this study are compiled in the documented R package
889 “seasonalclumped”, which is freely available on the open-source online R-database CRAN (de Winter,
890 2021a; <https://cran.r-project.org/web/packages/seasonalclumped>). Annotated R scripts used to make
891 calculations for this study are available in the digital supplement uploaded to the open-source online
892 repository Zenodo (www.doi.org/10.5281/zenodo.3899926).

893

894 **Data availability**

895 Supplementary data, figures and tables as well as all scripts used to do the calculations and create the
896 virtual datasets used in this study are deposited in the open-source online repository Zenodo
897 (www.doi.org/10.5281/zenodo.3899926). Virtual datasets generated within the context of this study are also
898 made available as datafiles within the R package that contains the scripts used for this study
899 (“seasonalclumped”; de Winter, 2021a; see <https://cran.r-project.org/web/packages/seasonalclumped>).

900

901 **Author contributions**

902 NJW designed the study, wrote the scripts for all calculations, and created a first draft of the manuscript
903 text and figures. MZ, TA and NJW worked together from the first draft towards the final manuscript. All
904 authors contributed to the representation of the data and methods in figures and to the discussion of the
905 implications of the data in the discussion.

906

907 **Competing Interests**

908 The authors have no potential conflicts of interest to declare with regards to this study.

909

910 **Acknowledgements**

911 The authors would like to thank editor Alberto Reyes for his helpful suggestions for improving the
912 manuscript and for moderating the review process. Thanks to Andrew Johnson and two anonymous
913 reviewers for their comments which helped improve the manuscript. All members of the Clumped Isotope
914 research group of Utrecht University, most notably Ilja Kocken and dr. Inigo Müller, are acknowledged for
915 their comments and recommendations on a presentation of the initial results of this study.

916

917 **Financial support**

918 NJW is funded by the European Commission through a Marie Skłodowska Curie Individual Fellowship
919 (UNBIAS, grant # 843011) and by the Flemish Research Council (FWO) through a Junior Postdoctoral
920 Fellowship (12ZB220N).

921

922 **References**

923 Bahr, K. D., Jokieli, P. L. and Rodgers, K. S.: Seasonal and annual calcification rates of the Hawaiian reef
924 coral, *Montipora capitata*, under present and future climate change scenarios, *ICES J Mar Sci*, 74(4),
925 1083–1091, <https://doi.org/10.1093/icesjms/fsw078>, 2017.

926 Bernasconi, S. M., Müller, I. A., Bergmann, K. D., Breitenbach, S. F., Fernandez, A., Hodell, D. A., Jaggi,
927 M., Meckler, A. N., Millan, I. and Ziegler, M.: Reducing uncertainties in carbonate clumped isotope
928 analysis through consistent carbonate-based standardization, *Geochemistry, Geophysics, Geosystems*,
929 19(9), 2895–2914, 2018.

930 Brand, W. A., Coplen, T. B., Vogl, J., Rosner, M. and Prohaska, T.: Assessment of international reference
931 materials for isotope-ratio analysis (IUPAC Technical Report), *Pure and Applied Chemistry*, 86(3), 425–
932 467, <https://doi.org/10.1515/pac-2013-1023>, 2014.

933 Briard, J., Pucéat, E., Vennin, E., Daëron, M., Chavagnac, V., Jaillet, R., Merle, D. and de Rafélis, M.:
934 Seawater paleotemperature and paleosalinity evolution in neritic environments of the Mediterranean
935 margin: Insights from isotope analysis of bivalve shells, *Palaeogeography, Palaeoclimatology,*
936 *Palaeoecology*, 543, 109582, <https://doi.org/10.1016/j.palaeo.2019.109582>, 2020.

- 937 Bowen, G.J. WaterIsotopes.org: <http://wateriso.utah.edu/waterisotopes/index.html>, last access: 28 July
938 2020.
- 939 Caldarescu, D. E., Sadatzki, H., Andersson, C., Schäfer, P., Fortunato, H. and Meckler, A. N.: Clumped
940 isotope thermometry in bivalve shells: A tool for reconstructing seasonal upwelling, *Geochimica et*
941 *Cosmochimica Acta*, 294, 174–191, <https://doi.org/10.1016/j.gca.2020.11.019>, 2021.
- 942 Charles, C. D., Hunter, D. E. and Fairbanks, R. G.: Interaction between the ENSO and the Asian monsoon
943 in a coral record of tropical climate, *Science*, 277(5328), 925–928, 1997.
- 944 Comboul, M., Emile-Geay, J., Evans, M. N., Mirnategui, N., Cobb, K. M. and Thompson, D. M.: A
945 probabilistic model of chronological errors in layer-counted climate proxies: applications to annually
946 banded coral archives, *Climate of the Past*, 10(2), 825–841, 2014.
- 947 Compton, T. J., Rijkenberg, M. J. A., Drent, J. and Piersma, T.: Thermal tolerance ranges and climate
948 variability: A comparison between bivalves from differing climates, *Journal of Experimental Marine*
949 *Biology and Ecology*, 352(1), 200–211, <https://doi.org/10.1016/j.jembe.2007.07.010>, 2007.
- 950 Cook, E. R. and Kairiukstis, L. A.: *Methods of dendrochronology: applications in the environmental*
951 *sciences*, Springer Science & Business Media., 2013.
- 952 Cramer, B. S., Toggweiler, J. R., Wright, J. D., Katz, M. E. and Miller, K. G.: Ocean overturning since the
953 Late Cretaceous: Inferences from a new benthic foraminiferal isotope compilation, *Paleoceanography*,
954 24(4), <https://doi.org/10.1029/2008PA001683>, 2009.
- 955 Crossland, C.: Seasonal variations in the rates of calcification and productivity in the coral *Acropora formosa*
956 on a high-latitude reef, *Marine Ecology Progress Series*, 15, 135–140,
957 <https://doi.org/10.3354/meps015135>, 1984.
- 958 Dattalo, P.: *Determining Sample Size: Balancing Power, Precision, and Practicality*, Oxford University
959 Press, USA., 2008.
- 960 Dayem, K. E., Molnar, P., Battisti, D. S. and Roe, G. H.: Lessons learned from oxygen isotopes in modern
961 precipitation applied to interpretation of speleothem records of paleoclimate from eastern Asia, *Earth and*
962 *Planetary Science Letters*, 295(1–2), 219–230, 2010.
- 963 De Ridder, F., de Brauwere, A., Pintelon, R., Schoukens, J., Dehairs, F., Baeyens, W. and Wilkinson, B.
964 H.: Comment on: Paleoclimatic inference from stable isotope profiles of accretionary biogenic hardparts—
965 a quantitative approach to the evaluation of incomplete data, by Wilkinson, B.H., Ivany, L.C., 2002.
966 *Palaeogeogr. Palaeocl. Palaeoecol.* 185, 95–114, *Palaeogeography, Palaeoclimatology, Palaeoecology*,
967 248(3–4), 473–476, <https://doi.org/10.1016/j.palaeo.2006.08.004>, 2007.
- 968 De Vleeschouwer, D., Vahlenkamp, M., Crucifix, M. and Pälike, H.: Alternating Southern and Northern
969 Hemisphere climate response to astronomical forcing during the past 35 my, *Geology*, 45(4), 375–378,
970 2017.
- 971 de Winter, N. J., Snoeck, C. and Claeys, P.: Seasonal Cyclicity in Trace Elements and Stable Isotopes of
972 Modern Horse Enamel, *PLoS one*, 11(11), e0166678, 2016.
- 973 de Winter, N., Sinnesael, M., Makarona, C., Vansteenberge, S. and Claeys, P.: Trace element analyses of
974 carbonates using portable and micro-X-ray fluorescence: Performance and optimization of measurement
975 parameters and strategies., *Journal of Analytical Atomic Spectrometry*, 32(6), 1211–1223,
976 <https://doi.org/10.1039/C6JA00361C>, 2017.

- 977 de Winter, N. J., Vellekoop, J., Vorsselmans, R., Golreihan, A., Soete, J., Petersen, S. V., Meyer, K. W.,
978 Casadio, S., Speijer, R. P. and Claeys, P.: An assessment of latest Cretaceous Pycnodonte vesicularis
979 (Lamarck, 1806) shells as records for palaeoseasonality: a multi-proxy investigation, *Climate of the Past*,
980 14(6), 725–749, 2018.
- 981 de Winter, N. J., Goderis, S., Malderen, S. J. M. V., Sinnesael, M., Vansteenberge, S., Snoeck, C., Belza,
982 J., Vanhaecke, F. and Claeys, P.: Subdaily-Scale Chemical Variability in a *Torreites Sanchezi* Rudist
983 Shell: Implications for Rudist Paleobiology and the Cretaceous Day-Night Cycle, *Paleoceanography and*
984 *Paleoclimatology*, 35(2), e2019PA003723, <https://doi.org/10.1029/2019PA003723>, 2020a.
- 985 de Winter, N. J., Müller, I. A., Kocken, I. J., Thibault, N., Ullmann, C. V., Farnsworth, A., Lunt, D. J., Claeys,
986 P. and Ziegler, M.: First absolute seasonal temperature estimates for greenhouse climate from clumped
987 isotopes in bivalve shells, *Nature Communications*, in review, <https://doi.org/10.21203/rs.3.rs-39203/v1>,
988 2020b.
- 989 de Winter, N. J., Ullmann, C. V., Sørensen, A. M., Thibault, N., Goderis, S., Van Malderen, S. J. M., Snoeck,
990 C., Goolaerts, S., Vanhaecke, F. and Claeys, P.: Shell chemistry of the boreal Campanian bivalve
991 *Rastellum diluvianum*; (Linnaeus, 1767) reveals temperature seasonality, growth rates and life cycle of
992 an extinct Cretaceous oyster, *Biogeosciences*, 17(11), 2897–2922, [https://doi.org/10.5194/bg-17-2897-](https://doi.org/10.5194/bg-17-2897-2020)
993 2020, 2020c.
- 994 de Winter, N. J., Vellekoop, J., Clark, A. J., Stassen, P., Speijer, R. P. and Claeys, P.: The giant marine
995 gastropod *Campanile giganteum* (Lamarck, 1804) as a high-resolution archive of seasonality in the
996 Eocene greenhouse world, *Geochemistry, Geophysics, Geosystems*, 21(n/a), e2019GC008794,
997 <https://doi.org/10.1029/2019GC008794>, 2020d.
- 998 de Winter, N. J.: seasonalclumped: Toolbox for Clumped Isotope Seasonality Reconstructions.
999 <https://CRAN.R-project.org/package=seasonalclumped>, last access: 4 February 2021, 2021a.
- 1000 de Winter, N. J.: ShellChron 0.2.8: A new tool for constructing chronologies in accretionary carbonate
1001 archives from stable oxygen isotope profiles, *Geoscientific Model Development Discussions*, 1–37,
1002 <https://doi.org/10.5194/gmd-2020-401>, 2021b.
- 1003 Denton, G. H., Alley, R. B., Comer, G. C. and Broecker, W. S.: The role of seasonality in abrupt climate
1004 change, *Quaternary Science Reviews*, 24(10), 1159–1182,
1005 <https://doi.org/10.1016/j.quascirev.2004.12.002>, 2005.
- 1006 Eiler, J. M.: Paleoclimate reconstruction using carbonate clumped isotope thermometry, 30, 3575–3588,
1007 2011.
- 1008 Fairbanks, R. G., Evans, M. N., Rubenstone, J. L., Mortlock, R. A., Broad, K., Moore, M. D. and Charles,
1009 C. D.: Evaluating climate indices and their geochemical proxies measured in corals, *Coral Reefs*, 16(1),
1010 S93–S100, <https://doi.org/10.1007/s003380050245>, 1997.
- 1011 Fernandez, A., Müller, I. A., Rodríguez-Sanz, L., van Dijk, J., Looser, N. and Bernasconi, S. M.: A
1012 reassessment of the precision of carbonate clumped isotope measurements: implications for calibrations
1013 and paleoclimate reconstructions, *Geochemistry, Geophysics, Geosystems*, 18(12), 4375–4386, 2017.
- 1014 Gaspar, M. B., Ferreira, R. and Monteiro, C. C.: Growth and reproductive cycle of *Donax trunculus* L.,
1015 (Mollusca: Bivalvia) off Faro, southern Portugal, *Fisheries Research*, 41(3), 309–316,
1016 [https://doi.org/10.1016/S0165-7836\(99\)00017-X](https://doi.org/10.1016/S0165-7836(99)00017-X), 1999.

- 1017 Goodwin, D. H., Schöne, B. R. and Dettman, D. L.: Resolution and fidelity of oxygen isotopes as
1018 paleotemperature proxies in bivalve mollusk shells: models and observations, *Palaios*, 18(2), 110–125,
1019 2003.
- 1020 Goodwin, D. H., Paul, P. and Wissink, C. L.: MoGroFunGen: A numerical model for reconstructing intra-
1021 annual growth rates of bivalve molluscs, *Palaeogeography, Palaeoclimatology, Palaeoecology*, 276(1),
1022 47–55, <https://doi.org/10.1016/j.palaeo.2009.02.026>, 2009.
- 1023 Harwood, A. J. P., Dennis, P. F., Marca, A. D., Pilling, G. M. and Millner, R. S.: The oxygen isotope
1024 composition of water masses within the North Sea, *Estuarine, Coastal and Shelf Science*, 78(2), 353–
1025 359, <https://doi.org/10.1016/j.ecss.2007.12.010>, 2008.
- 1026 Hendriks, I. E., Basso, L., Deudero, S., Cabanellas-Reboredo, M. and Álvarez, E.: Relative growth rates of
1027 the noble pen shell *Pinna nobilis* throughout ontogeny around the Balearic Islands (Western
1028 Mediterranean, Spain), *Journal of Shellfish Research*, 31(3), 749–756, 2012.
- 1029 Henkes, G. A., Passey, B. H., Grossman, E. L., Shenton, B. J., Yancey, T. E. and Pérez-Huerta, A.:
1030 Temperature evolution and the oxygen isotope composition of Phanerozoic oceans from carbonate
1031 clumped isotope thermometry, *Earth and Planetary Science Letters*, 490, 40–50,
1032 <https://doi.org/10.1016/j.epsl.2018.02.001>, 2018.
- 1033 Hurrell, J. W.: Decadal trends in the North Atlantic Oscillation: regional temperatures and precipitation,
1034 *Science*, 269(5224), 676–679, 1995.
- 1035 Huybers, P. and Curry, W.: Links between annual, Milankovitch and continuum temperature variability,
1036 *Nature*, 441(7091), 329, 2006.
- 1037 Huyghe, D., Lartaud, F., Emmanuel, L., Merle, D. and Renard, M.: Palaeogene climate evolution in the
1038 Paris Basin from oxygen stable isotope ($\delta^{18}\text{O}$) compositions of marine molluscs, *Journal of the
1039 Geological Society*, 172(5), 576–587, 2015.
- 1040 Huyghe, D., de Rafélis, M., Ropert, M., Mouchi, V., Emmanuel, L., Renard, M. and Lartaud, F.: New insights
1041 into oyster high-resolution hinge growth patterns, *Marine biology*, 166(4), 48, 2019.
- 1042 IPCC: IPCC, 2013: Climate Change 2013: The Physical Science Basis. Contribution of Working Group I to
1043 the Fifth Assessment Report of the Intergovernmental Panel on Climate Change, 1535 pp, Cambridge
1044 Univ. Press, Cambridge, UK, and New York., 2013.
- 1045 Ivany, L. C.: Reconstructing paleoseasonality from accretionary skeletal carbonates—challenges and
1046 opportunities, *The Paleontological Society Papers*, 18, 133–166, 2012.
- 1047 Jaffrés, J. B. D., Shields, G. A., and Wallmann, K.: The oxygen isotope evolution of seawater: A critical
1048 review of a long-standing controversy and an improved geological water cycle model for the past 3.4
1049 billion years, *Earth-Science Reviews*, 83, 83–122, <https://doi.org/10.1016/j.earscirev.2007.04.002>, 2007.
- 1050 Jenkyns, H. C.: Geochemistry of oceanic anoxic events, *Geochemistry, Geophysics, Geosystems*, 11(3),
1051 <https://doi.org/10.1029/2009GC002788>, 2010.
- 1052 Johnson, A. L. A., Valentine, A. M., Leng, M. J., Schöne, B. R., and Sloane, H. J.: Life history, environment
1053 and extinction of the scallop *Carolinapecten eboreus* (Conrad) In the Plio-Pleistocene of the U.S. eastern
1054 seaboard, *PALAIOS*, 34, 49–70, <https://doi.org/10.2110/palo.2018.056>, 2019.

- 1055 Jones, A. M., Iacumin, P. and Young, E. D.: High-resolution d18O analysis of tooth enamel phosphate by
1056 isotope ratio monitoring gas chromatography mass spectrometry and ultraviolet laser fluorination, , 8,
1057 1999.
- 1058 Judd, E. J., Wilkinson, B. H. and Ivany, L. C.: The life and time of clams: Derivation of intra-annual growth
1059 rates from high-resolution oxygen isotope profiles, *Palaeogeography, Palaeoclimatology, Palaeoecology*,
1060 490, 70–83, 2018.
- 1061 Keating-Bitonti, C. R., Ivany, L. C., Affek, H. P., Douglas, P. and Samson, S. D.: Warm, not super-hot,
1062 temperatures in the early Eocene subtropics, *Geology*, 39(8), 771–774,
1063 <https://doi.org/10.1130/G32054.1>, 2011.
- 1064 Kele, S., Breitenbach, S. F., Capezzuoli, E., Meckler, A. N., Ziegler, M., Millan, I. M., Kluge, T., Deák, J.,
1065 Hanselmann, K. and John, C. M.: Temperature dependence of oxygen-and clumped isotope fractionation
1066 in carbonates: a study of travertines and tufas in the 6–95 C temperature range, *Geochimica et*
1067 *Cosmochimica Acta*, 168, 172–192, 2015.
- 1068 Kim, S.-T. and O’Neil, J. R.: Equilibrium and nonequilibrium oxygen isotope effects in synthetic carbonates,
1069 *Geochimica et Cosmochimica Acta*, 61(16), 3461–3475, [https://doi.org/10.1016/S0016-7037\(97\)00169-](https://doi.org/10.1016/S0016-7037(97)00169-5)
1070 5, 1997.
- 1071 Kocken, I. J., Müller, I. A. and Ziegler, M.: Optimizing the Use of Carbonate Standards to Minimize
1072 Uncertainties in Clumped Isotope Data, *Geochemistry, Geophysics, Geosystems*, 20(11), 5565–5577,
1073 <https://doi.org/10.1029/2019GC008545>, 2019.
- 1074 Kohn, M. J.: Comment: tooth enamel mineralization in ungulates: implications for recovering a primary
1075 isotopic time-series, by BH Passey and TE Cerling (2002), *Geochimica et Cosmochimica Acta*, 68(2),
1076 403–405, 2004.
- 1077 Lauretano, V., Zachos, J. C. and Lourens, L. J.: Orbitally Paced Carbon and Deep-Sea Temperature
1078 Changes at the Peak of the Early Eocene Climatic Optimum, *Paleoceanography and Paleoclimatology*,
1079 33(10), 1050–1065, <https://doi.org/10.1029/2018PA003422>, 2018.
- 1080 Lear, C. H., Bailey, T. R., Pearson, P. N., Coxall, H. K. and Rosenthal, Y.: Cooling and ice growth across
1081 the Eocene-Oligocene transition, *Geology*, 36(3), 251–254, 2008.
- 1082 LeGrande, A. N. and Schmidt, G. A.: Global gridded data set of the oxygen isotopic composition in
1083 seawater, *Geophysical research letters*, 33(12), 2006.
- 1084 Lisiecki, L. E. and Raymo, M. E.: A Pliocene-Pleistocene stack of 57 globally distributed benthic $\delta^{18}\text{O}$
1085 records, *Paleoceanography*, 20(1), <https://doi.org/10.1029/2004PA001071>, 2005.
- 1086 Lourens, L. J., Becker, J., Bintanja, R., Hilgen, F. J., Tuenter, E., Van de Wal, R. S. and Ziegler, M.: Linear
1087 and non-linear response of late Neogene glacial cycles to obliquity forcing and implications for the
1088 Milankovitch theory, *Quaternary Science Reviews*, 29(1–2), 352–365, 2010.
- 1089 McArthur, J. M., Howarth, R. J. and Shields, G. A.: Strontium isotope stratigraphy, *The geologic time scale*,
1090 1, 127–144, 2012.
- 1091 Meckler, A. N., Ziegler, M., Millán, M. I., Breitenbach, S. F. and Bernasconi, S. M.: Long-term performance
1092 of the Kiel carbonate device with a new correction scheme for clumped isotope measurements, *Rapid*
1093 *Communications in Mass Spectrometry*, 28(15), 1705–1715, 2014.

- 1094 Merz, B. and Thieken, A. H.: Separating natural and epistemic uncertainty in flood frequency analysis,
1095 *Journal of Hydrology*, 309(1–4), 114–132, 2005.
- 1096 Meyers, S. R.: Astrochron: An R package for astrochronology, [http://cran.r-](http://cran.r-project.org/package=astrochron)
1097 [project.org/package=astrochron](http://cran.r-project.org/package=astrochron).
1098 <http://scholar.google.com/scholar?cluster=14876361610707754388&hl=en&oi=scholar>, last access: 30
1099 May 2017, 2014.
- 1100 Meyers, S. R.: Cyclostratigraphy and the problem of astrochronologic testing, *Earth-Science Reviews*, 190,
1101 190–223, <https://doi.org/10.1016/j.earscirev.2018.11.015>, 2019.
- 1102 Miyaji, T., Tanabe, K., Matsushima, Y., Sato, S., Yokoyama, Y. and Matsuzaki, H.: Response of daily and
1103 annual shell growth patterns of the intertidal bivalve *Phacosoma japonicum* to Holocene coastal climate
1104 change in Japan, *Palaeogeography, Palaeoclimatology, Palaeoecology*, 286(3), 107–120,
1105 <https://doi.org/10.1016/j.palaeo.2009.11.032>, 2010.
- 1106 Mook, W. G.: Stable carbon and oxygen isotopes of natural waters in the Netherlands, *Isotope hydrology*,
1107 1970, 163–190, 1970.
- 1108 Morgan, V. and van Ommen, T. D.: Seasonality in late-Holocene climate from ice-core records, *The*
1109 *Holocene*, 7(3), 351–354, <https://doi.org/10.1177/095968369700700312>, 1997.
- 1110 Mosley-Thompson, E., Thompson, L. G., Dai, J., Davis, M. and Lin, P. N.: Climate of the last 500 years:
1111 High resolution ice core records, *Quaternary Science Reviews*, 12(6), 419–430,
1112 [https://doi.org/10.1016/S0277-3791\(05\)80006-X](https://doi.org/10.1016/S0277-3791(05)80006-X), 1993.
- 1113 Müller, I. A., Fernandez, A., Radke, J., van Dijk, J., Bowen, D., Schwieters, J. and Bernasconi, S. M.:
1114 Carbonate clumped isotope analyses with the long-integration dual-inlet (LIDI) workflow: scratching at
1115 the lower sample weight boundaries: LIDI as key for more precise analyses on much less carbonate
1116 material, *Rapid Communications in Mass Spectrometry*, 31(12), 1057–1066,
1117 <https://doi.org/10.1002/rcm.7878>, 2017.
- 1118 Noorbergen, L. J., Abels, H. A., Hilgen, F. J., Robson, B. E., Jong, E. de, Dekkers, M. J., Krijgsman, W.,
1119 Smit, J., Collinson, M. E. and Kuiper, K. F.: Conceptual models for short-eccentricity-scale climate control
1120 on peat formation in a lower Palaeocene fluvial system, north-eastern Montana (USA), *Sedimentology*,
1121 65(3), 775–808, <https://doi.org/10.1111/sed.12405>, 2018.
- 1122 O'Brien, C. L., Robinson, S. A., Pancost, R. D., Sinninghe Damsté, J. S., Schouten, S., Lunt, D. J., Alsenz,
1123 H., Bornemann, A., Bottini, C., Brassell, S. C., Farnsworth, A., Forster, A., Huber, B. T., Inglis, G. N.,
1124 Jenkyns, H. C., Linnert, C., Littler, K., Markwick, P., McAnena, A., Mutterlose, J., Naafs, B. D. A.,
1125 Püttmann, W., Sluijs, A., van Helmond, N. A. G. M., Vellekoop, J., Wagner, T., and Wrobel, N. E.:
1126 Cretaceous sea-surface temperature evolution: Constraints from TEX 86 and planktonic foraminiferal
1127 oxygen isotopes, 172, 224–247, <https://doi.org/10.1016/j.earscirev.2017.07.012>, 2017.
- 1128 O'Donnell, M. S. and Ignizio, D. A.: Bioclimatic predictors for supporting ecological applications in the
1129 conterminous United States, *US Geological Survey Data Series*, 691(10), 2012.
- 1130 Passey, B. H. and Cerling, T. E.: Tooth enamel mineralization in ungulates: implications for recovering a
1131 primary isotopic time-series, *Geochimica et Cosmochimica Acta*, 66(18), 3225–3234, 2002.
- 1132 Petersen, S. V., Tabor, C. R., Lohmann, K. C., Poulsen, C. J., Meyer, K. W., Carpenter, S. J., Erickson, J.
1133 M., Matsunaga, K. K., Smith, S. Y. and Sheldon, N. D.: Temperature and salinity of the Late Cretaceous
1134 western interior seaway, *Geology*, 44(11), 903–906, 2016.

- 1135 Philander, S. G. H.: El Niño southern oscillation phenomena, *Nature*, 302(5906), 295–301, 1983.
- 1136 R Core Team: R: A language and environment for statistical computing. R Foundation for Statistical
1137 Computing, Vienna, Austria. <http://www.R-project.org/>, 2013.
- 1138 Rodríguez-Sanz, L., Bernasconi, S. M., Marino, G., Heslop, D., Müller, I. A., Fernandez, A., Grant, K. M.
1139 and Rohling, E. J.: Penultimate deglacial warming across the Mediterranean Sea revealed by clumped
1140 isotopes in foraminifera, *Scientific Reports*, 7(1), 1–11, <https://doi.org/10.1038/s41598-017-16528-6>,
1141 2017.
- 1142 Rohling, E. J.: Oxygen isotope composition of seawater, *The Encyclopedia of Quaternary Science*.
1143 Amsterdam: Elsevier, 2, 915–922, 2013.
- 1144 Sano, Y., Kobayashi, S., Shirai, K., Takahata, N., Matsumoto, K., Watanabe, T., Sowa, K. and Iwai, K.:
1145 Past daily light cycle recorded in the strontium/calcium ratios of giant clam shells, *Nature*
1146 *Communications*, 3, 761, 2012.
- 1147 Sato, S.: Temporal change of life-history traits in fossil bivalves: an example of *Phacosoma japonicum* from
1148 the Pleistocene of Japan, *Palaeogeography, Palaeoclimatology, Palaeoecology*, 154(4), 313–323,
1149 [https://doi.org/10.1016/S0031-0182\(99\)00106-6](https://doi.org/10.1016/S0031-0182(99)00106-6), 1999.
- 1150 Schmitt, J., Schneider, R., Elsig, J., Leuenberger, D., Lourantou, A., Chappellaz, J., Kohler, P., Joos, F.,
1151 Stocker, T. F., Leuenberger, M. and Fischer, H.: Carbon Isotope Constraints on the Deglacial CO₂ Rise
1152 from Ice Cores, *Science*, 336(6082), 711–714, <https://doi.org/10.1126/science.1217161>, 2012.
- 1153 Scholz, D. and Hoffmann, D. L.: StalAge—An algorithm designed for construction of speleothem age models,
1154 *Quaternary Geochronology*, 6(3–4), 369–382, 2011.
- 1155 Schöne, B. R.: The curse of physiology—challenges and opportunities in the interpretation of geochemical
1156 data from mollusk shells, *Geo-Marine Letters*, 28(5–6), 269–285, 2008.
- 1157 Schöne, B. R., Fiebig, J., Pfeiffer, M., Gleß, R., Hickson, J., Johnson, A. L., Dreyer, W. and Oschmann, W.:
1158 Climate records from a bivalved *Methuselah* (*Arctica islandica*, Mollusca; Iceland), *Palaeogeography,*
1159 *Palaeoclimatology, Palaeoecology*, 228(1–2), 130–148, 2005.
- 1160 Schöne, B. R., Rodland, D. L., Fiebig, J., Oschmann, W., Goodwin, D., Flessa, K. W. and Dettman, D.:
1161 Reliability of multitaxon, multiproxy reconstructions of environmental conditions from accretionary
1162 biogenic skeletons, *The Journal of geology*, 114(3), 267–285, 2006.
- 1163 Scourse, J., Richardson, C., Forsythe, G., Harris, I., Heinemeier, J., Fraser, N., Briffa, K. and Jones, P.:
1164 First cross-matched floating chronology from the marine fossil record: data from growth lines of the long-
1165 lived bivalve mollusc *Arctica islandica*, *The Holocene*, 16(7), 967–974,
1166 <https://doi.org/10.1177/0959683606h1987rp>, 2006.
- 1167 Sha, L., Mahata, S., Duan, P., Luz, B., Zhang, P., Baker, J., Zong, B., Ning, Y., Brahim, Y. A., Zhang, H.,
1168 Edwards, R. L. and Cheng, H.: A novel application of triple oxygen isotope ratios of speleothems,
1169 *Geochimica et Cosmochimica Acta*, 270, 360–378, <https://doi.org/10.1016/j.gca.2019.12.003>, 2020.
- 1170 Shao, D., Mei, Y., Yang, Z., Wang, Y., Yang, W., Gao, Y., Yang, L. and Sun, L.: Holocene ENSO variability
1171 in the South China Sea recorded by high-resolution oxygen isotope records from the shells of *Tridacna*
1172 spp., *Scientific Reports*, 10(1), 3921, <https://doi.org/10.1038/s41598-020-61013-2>, 2020.

- 1173 Sinnesael, M., De Vleeschouwer, D., Zeeden, C., Batenburg, S. J., Da Silva, A.-C., de Winter, N. J.,
1174 Dinarès-Turell, J., Drury, A. J., Gambacorta, G. and Hilgen, F. J.: The Cyclostratigraphy Intercomparison
1175 Project (CIP): consistency, merits and pitfalls, *Earth-Science Reviews*, 102965, 2019.
- 1176 Stap, L., Lourens, L. J., Thomas, E., Sluijs, A., Bohaty, S. and Zachos, J. C.: High-resolution deep-sea
1177 carbon and oxygen isotope records of Eocene Thermal Maximum 2 and H2, *Geology*, 38(7), 607–610,
1178 2010.
- 1179 Steffensen, J. P., Andersen, K. K., Bigler, M., Clausen, H. B., Dahl-Jensen, D., Fischer, H., Goto-Azuma,
1180 K., Hansson, M., Johnsen, S. J. and Jouzel, J.: High-resolution Greenland ice core data show abrupt
1181 climate change happens in few years, *Science*, 321(5889), 680–684, 2008.
- 1182 Steuber, T., Rauch, M., Masse, J.-P., Graaf, J. and Malkoč, M.: Low-latitude seasonality of Cretaceous
1183 temperatures in warm and cold episodes, *Nature*, 437(7063), 1341–1344,
1184 <https://doi.org/10.1038/nature04096>, 2005.
- 1185 Surge, D., Lohmann, K. C. and Dettman, D. L.: Controls on isotopic chemistry of the American oyster,
1186 *Crassostrea virginica*: implications for growth patterns, *Palaeogeography, Palaeoclimatology,*
1187 *Palaeoecology*, 172(3), 283–296, 2001.
- 1188 Tagliavento, M., John, C. M., and Stemmerik, L.: Tropical temperature in the Maastrichtian Danish Basin:
1189 Data from coccolith $\Delta 47$ and $\delta 18O$, 47, 1074–1078, 2019.
- 1190 Titschack, J., Zuschin, M., Spötl, C. and Baal, C.: The giant oyster *Hytotissa hyotis* from the northern Red
1191 Sea as a decadal-scale archive for seasonal environmental fluctuations in coral reef habitats, *Coral*
1192 *Reefs*, 29(4), 1061–1075, 2010.
- 1193 Treble, P., Shelley, J. M. G. and Chappell, J.: Comparison of high resolution sub-annual records of trace
1194 elements in a modern (1911–1992) speleothem with instrumental climate data from southwest Australia,
1195 *Earth and Planetary Science Letters*, 216(1), 141–153, [https://doi.org/10.1016/S0012-821X\(03\)00504-1](https://doi.org/10.1016/S0012-821X(03)00504-1),
1196 2003.
- 1197 Tsukakoshi, Y.: Sampling variability and uncertainty in total diet studies, *Analyst*, 136(3), 533–539,
1198 <https://doi.org/10.1039/C0AN00397B>, 2011.
- 1199 Tudhope, A. W.: Variability in the El Nino-Southern Oscillation Through a Glacial-Interglacial Cycle,
1200 *Science*, 291(5508), 1511–1517, <https://doi.org/10.1126/science.1057969>, 2001.
- 1201 Ullmann, C. V., Wiechert, U. and Korte, C.: Oxygen isotope fluctuations in a modern North Sea oyster
1202 (*Crassostrea gigas*) compared with annual variations in seawater temperature: Implications for
1203 palaeoclimate studies, *Chemical Geology*, 277(1), 160–166, 2010.
- 1204 van Dam, J. A. and Reichart, G. J.: Oxygen and carbon isotope signatures in late Neogene horse teeth
1205 from Spain and application as temperature and seasonality proxies, *Palaeogeography,*
1206 *Palaeoclimatology, Palaeoecology*, 274(1–2), 64–81, <https://doi.org/10.1016/j.palaeo.2008.12.022>,
1207 2009.
- 1208 Van Rampelbergh, M., Verheyden, S., Allan, M., Quinif, Y., Keppens, E. and Claeys, P.: Seasonal variations
1209 recorded in cave monitoring results and a 10 year monthly resolved speleothem $\delta 18O$ and $\delta 13C$ record
1210 from the Han-sur-Lesse cave, Belgium, *Climate of the Past Discussions*, 10, 1821–1856, 2014.

- 1211 Vansteenberge, S., Verheyden, S., Cheng, H., Edwards, R. L., Keppens, E. and Claeys, P.: Paleoclimate
 1212 in continental northwestern Europe during the Eemian and early Weichselian (125–97 ka): insights from
 1213 a Belgian speleothem, *Clim. Past*, 12(7), 1445–1458, <https://doi.org/10.5194/cp-12-1445-2016>, 2016.
- 1214 Vansteenberge, S., Winter, N. de, Sinnesael, M., Verheyden, S., Goderis, S., Malderen, S. J. M. V.,
 1215 Vanhaecke, F. and Claeys, P.: Reconstructing seasonality through stable isotope and trace element
 1216 analysis of the Proserpine stalagmite, Han-sur-Lesse Cave, Belgium: indications for climate-driven
 1217 changes during the last 400 years, *Climate of the Past Discussions*, 1–32, [https://doi.org/10.5194/cp-](https://doi.org/10.5194/cp-2019-78)
 1218 2019-78, 2019.
- 1219 Veizer, J. and Prokoph, A.: Temperatures and oxygen isotopic composition of Phanerozoic oceans, *Earth-*
 1220 *Science Reviews*, 146, 92–104, <https://doi.org/10.1016/j.earscirev.2015.03.008>, 2015.
- 1221 Vleeschouwer, D. D., Vahlenkamp, M., Crucifix, M. and Pälike, H.: Alternating Southern and Northern
 1222 Hemisphere climate response to astronomical forcing during the past 35 m.y., *Geology*, 45(4), 375–378,
 1223 <https://doi.org/10.1130/G38663.1>, 2017.
- 1224 Warter, V. and Müller, W.: Daily growth and tidal rhythms in Miocene and modern giant clams revealed via
 1225 ultra-high resolution LA-ICPMS analysis—A novel methodological approach towards improved
 1226 sclerochemistry, *Palaeogeography, Palaeoclimatology, Palaeoecology*, 465, 362–375, 2017.
- 1227 Westerhold, T., Marwan, N., Drury, A. J., Liebrand, D., Agnini, C., Anagnostou, E., Barnet, J. S., Bohaty,
 1228 S. M., De Vleeschouwer, D. and Florindo, F.: An astronomically dated record of Earth’s climate and its
 1229 predictability over the last 66 million years, *Science*, 369(6509), 1383–1387, 2020.
- 1230 Wilkinson, B. H. and Ivany, L. C.: Paleoclimatic inference from stable isotope profiles of accretionary
 1231 biogenic hardparts – a quantitative approach to the evaluation of incomplete data, *Palaeogeography,*
 1232 *Palaeoclimatology, Palaeoecology*, 185(1), 95–114, [https://doi.org/10.1016/S0031-0182\(02\)00279-1](https://doi.org/10.1016/S0031-0182(02)00279-1),
 1233 2002.
- 1234 Williams, M., Haywood, A. M., Harper, E. M., Johnson, A. L. A., Knowles, T., Leng, M. J., Lunt, D. J.,
 1235 Okamura, B., Taylor, P. D., and Zalasiewicz, J.: Pliocene climate and seasonality in North Atlantic shelf
 1236 seas, *Philosophical Transactions of the Royal Society A: Mathematical, Physical and Engineering*
 1237 *Sciences*, 367, 85–108, <https://doi.org/10.1098/rsta.2008.0224>, 2009.
- 1238 Yan, H., Liu, C., An, Z., Yang, W., Yang, Y., Huang, P., Qiu, S., Zhou, P., Zhao, N. and Fei, H.: Extreme
 1239 weather events recorded by daily to hourly resolution biogeochemical proxies of marine giant clam shells,
 1240 *Proceedings of the National Academy of Sciences*, 2020.
- 1241 Zhang, L., Tang Wilson H., Zhang Lulu, and Zheng Jianguo: Reducing Uncertainty of Prediction from
 1242 Empirical Correlations, *Journal of Geotechnical and Geoenvironmental Engineering*, 130, 526–534,
 1243 [https://doi.org/10.1061/\(ASCE\)1090-0241\(2004\)130:5\(526\)](https://doi.org/10.1061/(ASCE)1090-0241(2004)130:5(526)), 2004.